ELSEVIER

Contents lists available at ScienceDirect

International Journal of Biological Macromolecules

journal homepage: www.elsevier.com/locate/ijbiomac





Immunometabolic interplay in *Edwardsiella tarda*-infected crucian carp (*Carassius auratus*) and *in vitro* identification of the antimicrobial activity of apolipoprotein D (ApoD) by utilization of multiomics analyses

Fei Wang ^{a,1}, Ning-Xia Xiong ^{b,1}, Jie Ou ^a, Zi-Rou Zhong ^a, Qing Xie ^a, Jin-Fang Huang ^a, Ke-Xin Li ^a, Ming-Zhu Huang ^c, Zi-Xuan Fang ^a, Xu-Ying Kuang ^a, Zi-Le Qin ^a, Sheng-Wei Luo ^{a,*}

- ^a State Key Laboratory of Developmental Biology of Freshwater Fish, Engineering Research Center of Polyploidy fish Reproduction and Breeding of the State Education Ministry, College of Life Science, Hunan Normal University, Changsha 410081, PR China
- b Department of Aquatic Animal Medicine, College of Fisheries, Huazhong Agricultural University, Wuhan 430070, PR China
- ^c National R&D Center for freshwater fish processing, Jiangxi Normal University, Nanchang 330022, PR China

ARTICLE INFO

Keywords: Crucian carp Immunometabolism ApoD Antimicrobial activity

ABSTRACT

Edwardsiella tarda is an intracellular pathogenic bacteria that can imperil the health of farmed fish. However, the interactive networks of immune regulation and metabolic response in *E. tarda*-infected fish are still unclear. In this investigation, we aimed to explore immunometabolic interplay in crucian carp after *E. tarda* infection by utilizing multiomics analyses. Crucian carp (*Carassius auratus*) receiving *E. tarda* infection showed increased levels of tissue damage and oxidative injury in liver. Multiomics analyses suggested that carbon and amino acid metabolism may be considered as crucial metabolic pathways in liver of crucian carp following *E. tarda* infection, while spaglumic acid, isocitric acid and tetrahydrocortisone were the crucial liver biomarkers. After that, a potential antimicrobial peptide (AMP) sequence called apolipoprotein D (ApoD) was identified from omics study. Then, tissue-specific analysis indicated that liver CaApoD showed the highest expression among isolated tissues. After *Aeromonas hydrophila* stimulated, CaApoD expressions increased sharply in immune-related tissues. Moreover, CaApoD fusion protein could mediate the *in vitro* binding to *A. hydrophila* and *E. tarda*, attenuate bacterial growth as well as diminish bacterial biofilm forming activity. These findings may have a comprehensive implication for understanding immunometabolic response in crucian carp upon infection.

1. Introduction

Crucian carp (*Carassius auratus*) is one of popular farmed fish species in China, which is due to its delicious taste and high stress tolerance [1]. Recent findings indicate that teleost fish contain a large quantity of immune regulators, such as pattern recognition receptors (PRRs), complement components and signal adaptors, playing pivotal roles in immune defense against invading bacteria [2]. However, some invading pathogens are able to suppress bactericidal response and evade host immune surveillance [3]. Whist invasive pathogens succeed in the breach of mucosal epithelial barriers, they can further aggravate infection processes at inflammatory foci [4]. In general, liver is one of predominant sites involved in detoxification, metabolic processes and immune response to invading pathogens, which is capable of generating

80 % to 90 % of complement components and pattern-recognition receptors [5,6]. Moreover, liver also acts as one of frontline immune organs that can receive gut-derived substances to activate immune response to circulating antigens and foreign endotoxins [7]. However, our previous findings indicated that the induction of inflammatory cytokine may lead to disorder of mucosal immune regulation and then aggravate tissue injury in gut-liver axis of crucian carp during bacterial infection [8,9]. Among known pathogens, *Edwardsiella tarda* is the etiologic agent of edwardsiellosis, which may cause a great economic loss in aquaculture [10].

Transcriptome is able to offer a global understanding of signal regulation with the real-time detection of gene profiles [11], while metabolome can systematically characterize the changes of endogenous metabolites involved in various biological processes [12]. To data,

 $^{^{\}star}$ Corresponding author.

E-mail address: swluo@hunnu.edu.cn (S.-W. Luo).

 $^{^{1}\,}$ These authors contributed equally to this work.

single-omics research cannot thoroughly account for the underlying pathogenesis of particular diseases, thus the multiomics application is in urgent need [13]. Immunometabolism is an emerging field of investigation linking immune regulation to metabolic process, which can provide a novel insight into the mechanism between infection-induced symptoms and innate/adaptive immune response [14]. Recent studies indicate that multiomics analyses not only provide a novel insight into pathogen-induced symptoms via immunometabolic signals, but also screen core genes or biomarkers for further functional investigation [15]. In contrast to antibiotics used in aquaculture, antimicrobial peptides (AMPs) are a diverse group of low-molecular-weight (LWC) peptides, which can exhibit the broad-spectrum antimicrobial activity without the development of resistant phenotype in pathogens [16,17]. AMPs can disrupt cell membranes of microorganisms by electrostatically interacting with the surface of negative-charged cell membranes or targeting to some specific membrane compounds [18,19]. Despite mammalian AMPs have been extensively studied, various forms of functional proteins with antibacterial activity in fish require further exploration. However, the immunometabolic interplay of E. tardainfected crucian carp and the potential antibacterial molecules are still

In this study, the aims were to evaluate pathological feature and antioxidant status in liver of crucian carp following *E. tarda* challenge. Then, integrated investigation of transcriptome and metabolome in liver were performed. Based on multiomics data, a novel sequence and domain structure of potential AMP called apolipoprotein D (ApoD) was identified in crucian carp. To further characterize its function, we also studied its antimicrobial role *in vitro*, which may provide a new insight to the immune regulation of hybrid fish.

2. Materials and methods

2.1. Ethical approval

All procedures, including the care and use of experimental fish, were approved by Animal Care and Use Committee of Hunan Normal University (Changsha City, Hunan province, China) and the Technical Committee for Laboratory Animal Sciences of the Standardisation Administration of China (SAC/TC281), and performed under the national standard Guidelines for Ethical Review of Animal Welfare (GB/T 35892-2018).

2.2. Animal preparation and experimental design

Healthy crucian carps (about 20.54 \pm 0.98 g) were collected from a fishing base (Changsha, China). Then, fish were daily fed with commercial diets and acclimatized in clean water (21–24 $^{\circ}\text{C}$, pH 7.6–8.2) of several water tanks till 24 h before infection experiment. Diet feed and feces were removed daily to avoid pathogenic contamination during the periods of fish acclimation and infection process. Before infection experiment, healthy crucian carps were randomly selected for determination of health status by PCR amplification using specific primers of virulence genes.

The diagram of animal groups and experiment design was shown in Fig. S1. In addition, the detailed information of pathogenic bacteria used in this study were presented in Table. S1. To investigate immunometabolic interplay in *E. tarda*-infected crucian carp, a total of 46 fish were randomly divided in several water tanks and sacrificed for tissue section, bacterial loads, biochemistry analysis and multiomics analyses. In brief, *E. tarda* was cultured in Luria-Bertani (LB) medium at 28 °C for 24 h and then resuspended in phosphate buffered saline (PBS, pH 7.3) before use. After that, fish infected with 100 μ L suspension of *E. tarda* in PBS (1 × 10⁷ CFU mL⁻¹) were used as infection group (CaET), while fish injected with 100 μ L of sterile PBS were used as control group (Cactl). Tissue samples were isolated at 24 h post-infection. Tissue section, bacterial load detection, biochemistry assay and transcriptome analysis contained

three biological replicates, whereas each group in metabolomics analysis contained six biological replicates.

According to omics data, open reading frame (ORF) sequence of $\it CaApoD$ was cloned from liver cDNA template of crucian carp by touchdown PCR assay. To evaluate comprehensive immune response of ApoD to various pathogenic bacteria, another important pathogen $\it A.~hydrophila$ was used. A total of 42 fish were randomly divided in several water tanks and sacrificed for expression analysis by qRT-PCR assay. In brief, $\it A.~hydrophila$ was cultured in LB medium at 28 °C for 24 h and then resuspended in PBS before use. Crucian carps receiving 100 μ L suspension of $\it A.~hydrophila$ in PBS (1 \times 10⁷ CFU mL⁻¹) were used as infection group. Equivalent volume of sterile PBS injection was used as control group. Tissues were isolated at 0, 6, 12, 24, 36 and 48 h postchallenge, frozen in liquid nitrogen and preserved in $\it -80$ °C. Each group contained three biological replicates.

2.3. Pathological section analysis

After treatment with Bouin solution, fixed liver samples were dehydrated in gradient alcohol (70 % ethanol, overnight; 80 %, 90 %, 95 % and 100 % ethanol, 15 min each; xylene + 100 % ethanol (1:1) and xylene, 30 min each), followed by paraffin infiltration and embedment. Based on the manufacturer's instructions, liver slices were stained by using a hematoxylin and eosin (HE) staining kit (Beyotime Biotechnology, China) [20]. Then, pathological sections were observed by using a light microscope (Leica DM 4000 with Leica Q Vin 3 program). This experiment possessed three biological repeats.

2.4. Biochemical measurement in liver

The isolated liver samples were homogenized on ice and then their protein concentrations were quantified by bicinchoninic acid (BCA) method [21]. According to the manufacturer's instructions, catalase (CAT) activity in liver was measured at absorbance of 405 nm by using a CAT enzyme activity kit (Nanjing Jiancheng Bioengineering Institute, China). Enzymatic results were shown as U of CAT activity per milligram of protein. Glutathione reductase (GR) activity in liver was detected at absorbance of 412 nm by using a GR enzymatic activity kit with DTNB (Beyotime Biotechnology, China). Enzymatic activity was shown as U of GR activity per gram of protein. Lactate dehydrogenase (LDH) activity in liver was measured at absorbance of 450 nm by using a LDH activity kit (Nanjing Jiancheng Bioengineering Institute, China). Enzymatic activity was shown as U of LDH per gram of protein. Succinate dehydrogenase (SDH) activity in liver was detected at absorbance of 600 nm by using a SDH enzymatic activity kit (Nanjing Jiancheng Bioengineering institute, China). Enzymatic activity was shown as U of SDH per milligram of protein. Alkaline phosphatase (AKP) activity in liver was detected at absorbance of 520 nm by using a AKP activity kit (Nanjing Jiancheng Bioengineering institute, China). Enzymatic activity was shown as U of AKP per milligram of protein. Aspartate transaminase (AST) activity in liver was measured at absorbance of 510 nm by using a AST activity kit (Nanjing Jiancheng Bioengineering institute, China). Enzymatic activity was shown as U of AST per gram of protein. This experiment possessed three biological repeats.

2.5. Multiomics research in liver

2.5.1. Functional annotation by RNA-seq

Total RNA was isolated from liver samples by using RNeasy Kit (Qiagen, Germany). Total RNA (RIN > 7.0, OD260/280 = 2.0 to 2.2) was enriched from each sample for cDNA construction and purified for PCR amplification by using Illumina HiSeq 2500 platform (Metware Biotechnology Co., Ltd., Wuhan, China). After that, clean reads with high quality were obtained after the removal of raw reads possessing adapter contaminants, reads with >10 % N and low-quality reads. Obtained clean reads were mapped to reference genome of red crucian carp

Table 1
Primer sequences used in this study.

| Primer names | Sequence direction (5' \rightarrow 3') | Use |
|------------------|---|--------|
| apoD-F | ATGGAGGCACTTCAGGTT | Clone |
| apoD-R | AAGGCATGTTGCTGCACA | Clone |
| p32-apoD-EcoRI-F | CCGGAATTCATGCAGACCATCAGCTCTG | Vector |
| p32-apoD-Xhol-R | CCGCTCGAGTTAATGATGATGATGATGATGAGGCATGCTGCTGCACA | Vector |
| apoD-qpcr-F | GCTTCATTGAGGGAACTGC | qPCR |
| apoD-qpcr-R | GGATTTGAGGATGCCTAACA | qPCR |
| 18S-qpcr-F | CGGAGGTTCGAAGACGATCA | qPCR |
| 18S-qpcr-R | GAGGTTTCCCGTGTTGAGTC | qPCR |
| ucp1-qpcr-F | CGCTCGCTCTACAACGGC | qPCR |
| ucp1-qpcr-R | GGGCTTGGAAACGAACCTT | qPCR |
| hect-qpcr-F | GTTTGAGGAGGTCTGTCGCA | qPCR |
| hect-qpcr-R | GTTTGGGCTGGAGGATTTTC | qPCR |
| uba5-qpcr-F | ACGGAGGACTTGAGGAGGG | qPCR |
| uba5-qpcr-R | CCATTGTGGTGGCAGACT | qPCR |
| lmptp-qpcr-F | CCCGTGGAAAGTCGGTATTG | qPCR |
| lmptp-qpcr-R | TTTGGTGACCTGTCGTGCC | qPCR |
| gal-qpcr-F | TCCTGGTGTTGGAGAATGGC | qPCR |
| gal-qpcr-R | GGTCCGTATCACAGCACTTGG | qPCR |
| hsc70-2-qpcr-F | CAAAGGATAACAACTTGCTGGG | qPCR |
| hsc70-2-qpcr-R | TGACCTCAATCTGGGGAACAC | qPCR |
| ccr6-qpcr-F | TTTATGAGCGTTACCAATCCG | qPCR |
| ccr6-qpcr-R | ATGGGCACCGCAGTTTTC | qPCR |
| coq10b-qpcr-F | GAAAGACAGTCGTGCGAGGTT | qPCR |
| coq10b-qpcr-R | CTGAGAAGATGCTGAAGGAGGA | qPCR |
| acc-qpcr-F | AACTGAAAGAATGGGTGGAACG | qPCR |
| acc-qpcr-R | TGGCAGAGGACAGAGGTGATG | qPCR |
| prmt1-qpcr-F | TCAAGGATAAGGTGGTTCTGGA | qPCR |
| prmt1-qpcr-R | TCTCGCATAAATGACCGTGTT | qPCR |
| map2b-qpcr-F | GCAGCACTGGGAAAGGCA | qPCR |
| map2b-qpcr-R | TCGCACAGAGGCGGGTAG | qPCR |
| gamt-qpcr-F | CTTCTCAAAGGGCGAAAACTG | qPCR |
| gamt-qpcr-R | TAGCCTCTGGAATACACCATCAT | qPCR |
| pemt-qpcr-F | GGGACAAACTGGACCTCTTCA | qPCR |
| pemt-qpcr-R | CTCCTCCTTCATCTCCTCGG | qPCR |
| odc1-qpcr-F | GGGCTCTGATGACACCAAACT | qPCR |
| odc1-qpcr-R | CCGCACTGCTCCACGATA | qPCR |
| dgat2-qpcr-F | CTTCCCAGCCGAAACTACATT | qPCR |
| dgat2-qpcr-R | AAGCCTCATTCTCACCAAACG | qPCR |

(Carassius auratus red variety) by HISAT software. Based on fragments per kilobase million (FPKM) values and principal component analysis (PCA), expressions of differentially expressed genes (DEGs) were quantified by DESeq2 software. The filtering criteria of DEG were set as $|\log 2FC| \geq 1$ and false discovery rate (FDR) < 0.05. Then, expression patterns of DEGs were evaluated by using K-means clustering analysis. Functional annotation of DEG was performed by using gene ontology (GO) database and Kyoto Encyclopedia of Genes and Genomes (KEGG) database.

2.5.2. Metabolite isolation and functional annotation by LC-MS/MS

After homogenization, filtrated liver samples were dried in vacuum and then their metabolite amounts were measured by using UPLC-QTOF-MS analysis in both positive and negative ion mode along with quality controls throughout the experimental run. Raw data were calculated by XCMS program (Metware Biotechnology Co., Ltd., Wuhan, China). After that, filtered data were shown with retention time (RT), ratio of mass/charge (m/z) and coefficient of variation (CV). After identification by metabolome database, metabolic results were validated by partial least squares-discriminant analysis (PLS-DA) and orthogonal partial least squares-discriminant analysis (OPLS-DA) models. The threshold of differential metabolite (DM) rank was set as below: variable importance in projection (VIP) ≥ 1 , p-value <0.05 and fold change (FC) > 1.5 or < 0.667. Then, DM contents were presented by heatmap analysis. Metabolic proximities of DMs were analyzed by Pearson correlation analysis. According to VIP values, the data distribution and probability density of crucial DMs were evaluated. After that, metabolic pathways of crucial DMs were determined by KEGG database. The changed levels of DMs in KEGG pathways were calculated by

differential abundance (DA) score.

2.5.3. Joint analyses of multiomics data

The integrated analyses of transcriptome and metabolome were validated by two-way orthogonal partial least squares (O2PLS) model. The threshold of correlation analysis between DEGs and DMs was set as below: coefficient value >0.8 or <-0.8, p-value <0.05. The relations between DEGs and DMs were calculated by canonical correlation analysis (CCA). The coexpression patterns of DEGs and DMs were analyzed by nine quadrant plot and correlation clustering heatmap, respectively. Then, functional annotation of DEGs and DMs were calculated by KEGG analysis. The correlation network diagram was conducted by Cytoscape and Visio software.

2.6. Bacterial load and gene expression validation

2.6.1. DNA isolation for bacterial load detection

Genomic DNA was isolated from the isolated tissues (liver, kidney, spleen and intestine) by using a tissue DNA extraction kit (Magen Biotechnology, China). Then, DNA concentration was adjusted to 100 ng/ μ L before use [22].

2.6.2. RNA extraction and cDNA synthesis

Total RNA was isolated from liver samples by using FastPure cell/tissue Total RNA isolation Kit v2 (Vazyme Biotech, China) and then treated with DNAase to avoid genomic DNA contamination [9]. After quality detection, 1000 ng of total RNA was used to synthesize cDNA templates by using MonScript $^{\text{TM}}$ RT III All-in-One Mix with dsNase (Monad, China).

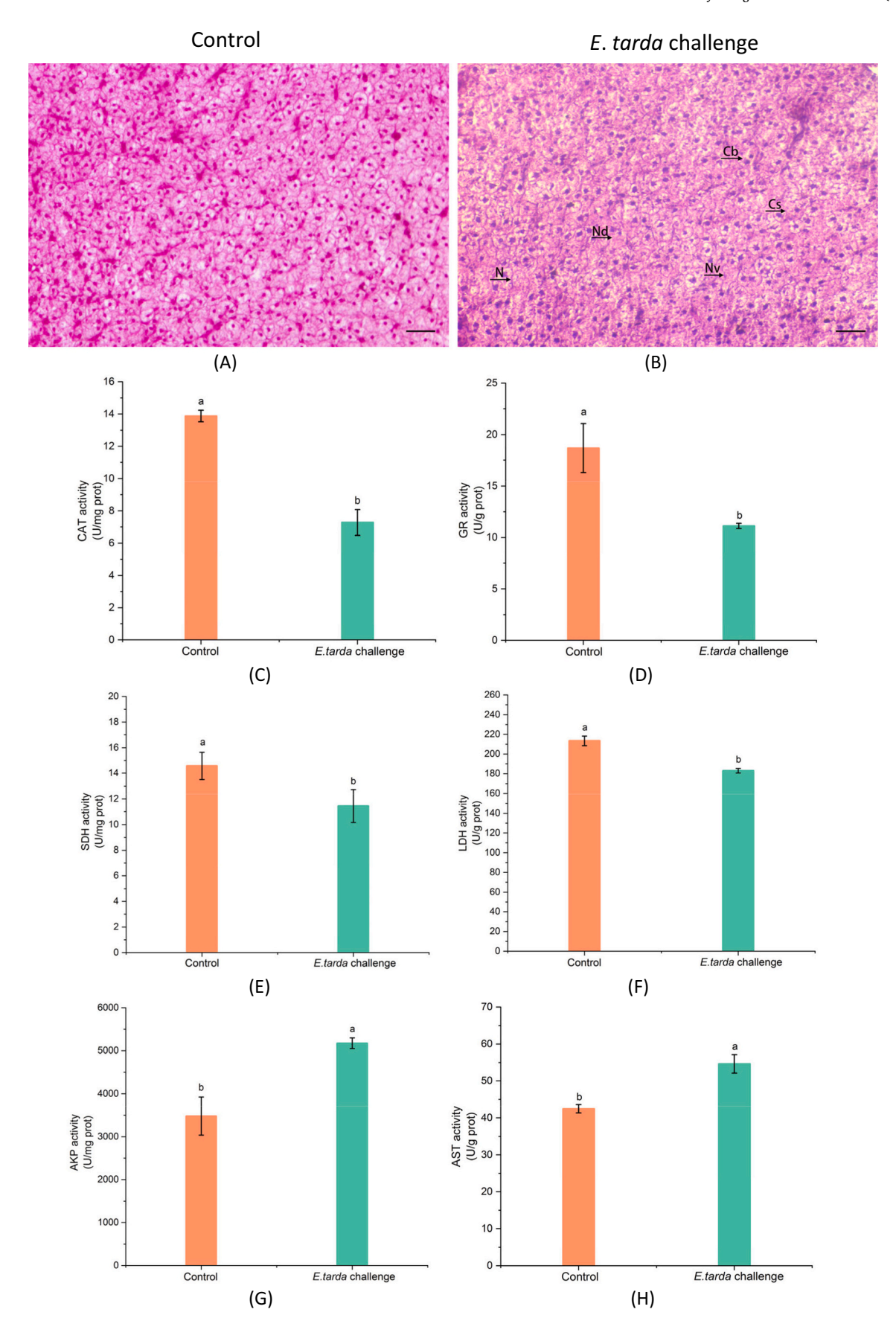


Fig. 1. Morphological analysis and antioxidant status in liver after *E. tarda* challenge. (A-B) Liver histological section. N: necrosis; Nd: nuclear displacement; Cb: cell boundary blurring; Nv: nuclear vanish; Cs: cell swelling. (C—H) Evaluation of crucial enzymatic markers in liver. The calculated data (mean \pm SD) with different letters were significantly different (P < 0.05).

2.6.3. Quantitative real-time PCR (qRT-PCR) assay

Relative expressions of E. tarda virulent gene and immunometabolic genes were evaluated by qRT-PCR assay [23]. For gene expression validation, relative expressions of uncoupling protein 1 (ucp1), homologous to the E6-AP carboxyl terminus (hect), ubiquitin-like modifieractivating enzyme 5 (uba5), low molecular weight phosphotyrosine protein phosphatase (Imptp), galactose-specific lectin (gal), heat shock cognate 70 kDa protein 2 (hsc70-2), CC motif chemokine receptor 6 (ccr6), coenzyme Q-binding protein COQ10 homolog B (coq10b), acetylcoA carboxylase (acc), probable protein arginine N-methyltransferase 1 (prmt1), methionine aminopeptidase 2B (map2b), guanidinoacetate Nmethyltransferase (gamt), phosphoethanolamine N-methyltransferase (pemt), ornithine decarboxylase 1 (odc1), diacylglycerol o-acyltransferase 2 (dgat2) and apolipoprotein D (ApoD) were measured in liver. 18S rRNA was used as reference gene. For bacterial load assay, relative expression of E. tarda mukf gene was detected in all isolated tissues, while gapdh gene was used as reference gene. According to the manufacturer's instructions, qRT-PCR reaction contained: 10.0 µL SYBR Green Master Mix (ABI), 2.0 μL DNA/cDNA template, 0.5 μL each primer and 7.0 µL ddH₂O. The program contained 1 cycle of 95 °C for 30s, 40 cycles of 95 °C for 15 s, 60 °C for 35 s, followed by 1 cycle of 95 °C for 30s, 60 °C for 60s. At the end of qRT-PCR amplified reaction, melting curve analysis was implemented to confirm the credibility of each qRT-PCR analysis. The primers were shown in Table. 1. This experiment possessed three biological repeats.

2.7. Identification and function analysis of CaApoD

2.7.1. Structure prediction of CaApoD

Structural motifs and binding sites of CaApoD were analyzed by National Center for Biotechnology Information (NCBI) blast program. Tertiary structure of CaApoD was calculated by phyre2 system. Binding sites on active clefts were screened by European Bioinformatics Institute (EMBL-EBI) database, while crucial domains in tertiary structure were analyzed by Mole system. Phylogenetic tree analysis was constructed by using MEGA 6.0 software and ITOL website (https://itol.embl.de/).

2.7.2. Prokaryotic expression, purification and validation of CaApoD

Generation of fusion protein was performed as previously described [24]. In brief, pET32 α and pET32 α -CaApoD plasmids were respectively transformed into E. coli BL21 clone. After screen of positive clones, bacteria were cultured in LB medium. When bacterial OD600 value reached about 0.6, isopropyl β-D-thiogalactoside (IPTG, 1 mM) was added into bacterial culture. Following another 4 h cultivation, bacteria were harvested for ultrasonication and the obtained pellets were dissolved in buffer. After that, purification of CaApoD fusion protein in supernatant was performed by using Ni-NTA Sefinose(TM) Resin 6FF (Sangon Biotech, China). According to protocols, active His bind resin was respectively loaded with $1 \times \text{binding buffer}$, soluble fusion protein solution, $1 \times$ binding buffer, $1 \times$ wash buffer and $1 \times$ elution buffer, respectively. After that, protein refolding process of purified CaApoD was performed at 4 °C by using dialysate containing gradient-decreased urea content. Then, purified CaApoD was separated and validated by western blotting assay. After incubation with His-tag primary antibody (GE healthcare) and alkaline phosphatase (AP)-conjugated secondary antibody (Beyotime Biotechnology, China), polyvinylidene fluoride (PVDF) membranes were visualized.

2.7.3. Bacterial binding activity of CaApoD

Bacterial binding activity of purified CaApoD protein was performed by Enzyme-linked immunosorbent assay (ELISA) as previously described [25]. When OD₆₀₀ value of *A. hydrophila* and *E. tarda* increased to approximately 0.8, bacteria numbers were adjusted to 1×10^7 CFU mL⁻¹. Then, ELISA plates were coated with above bacteria at 4 °C overnight, respectively. After blocking, ELISA plates were incubated with various doses of purified proteins at room temperature, followed by

incubation with anti-His antibody (GE healthcare) and horseradish peroxidase (HRP)-conjugated secondary antibody (Beyotime Biotechnology, China). After that, ELISA reaction was developed by using a highly sensitive TMB color solution kit (Beyotime Biotechnology, China). Binding index was calculated as follows: OD_{450} values in CaApoD group/ OD_{450} values in pET32a tag group (n=3).

2.7.4. Inhibition of biofilm formation by CaApoD

Inhibitory assay of biofilm formation by purified CaApoD protein was performed as previously described [26]. In brief, cocultivation of bacteria (A. hydrophila or E. tarda, 2×10^5 CFU mL $^{-1}$) and purified proteins (pet32a tag or CaApoD, 30.0 μg) were carried out at 28 °C overnight. After PBS wash, pathogenic biofilm was stained by using crystal violet method. After dissolving with ethanol, the mixed liquid was measured at OD570 nm. OD570 values of bacterial biofilm treated with purified CaApoD were recorded as A_{test} , while OD570 values of bacterial biofilm treated with pet32a tag were recorded as A_{ctl} . This experiment possessed three biological repeats. Inhibition rate of biofilm formation (%) = (1 - A_{test} / A_{ctl}) \times 100 %.

2.7.5. Antimicrobial activity of CaApoD

To investigate the antimicrobial effect of CaApoD on bacterial growth, the optical density measurement was performed as previously described [27]. Briefly, 10 μL of bacterial suspension (A. hydrophila or E. tarda, 2×10^5 CFU mL $^{-1}$) was incubated with 30 μg of purified proteins in a total volume of 600 μL at room temperature for 2 h. Following wash with PBS, the above mixtures were incubated in LB medium in a volume of 10 mL at 28 °C. The experiment was repeated in triplicate. Bacterial growth rate (%) was calculated as follows: OD_600 values in CaApoD group / OD_600 values in pET32a tag group \times 100 %.

2.8. Statistical analyses

The qRT-PCR results and enzymatic activities were subjected to one-way ANOVA or t-test analysis by using SPSS 17.0 software. Then, data visualization was operated by utilization of Origin 2022 program. The omics data was calculated and visualized by using cloud platform tools of Metware Biotechnology Co., Ltd. (https://cloud.metware.cn/). If the analytical levels reach <0.05 p-value, results were statistically significant.

3. Results

3.1. Determination of pathological condition after E. tarda infection

In order to assess the infectious status of crucian carp after $E.\ tarda$ infection, bacterial load assay was performed. Fish receiving bacterial infection exhibited 2.66-, 2.31-, 5.75- and 1.76-fold increased expression of $E.\ tarda$ mukf gene were observed in liver, kidney, spleen and intestine (p < 0.05) (Fig. S2). Then, tissue injury levels were determined by tissue section assay and crucial enzymatic activity. In Fig. 1A-B, an increased level of deformed morphology was observed in liver of crucian carp after $E.\ tarda$ challenge. $E.\ tarda$ infection could induce various ranges of tissue injury in liver of crucian carp, including necrosis (N), nuclear displacement (Nd), cell boundary blurring (Cb), nuclear vanish (Nv) and cell swelling (Cs). Disease- and redox-related parameters in liver following $E.\ tarda$ challenge were shown in Fig. 1C-H. Enzymatic activity of CAT, GR, SDH and LDH decreased by 1.90-, 1.68-, 1.27- and 1.17-fold in liver of crucian carp following $E.\ tarda$ challenge, whereas 1.49- and 1.29-fold increase of AKP and AST activity were observed (p < 0.05).

3.2. Liver transcripts determined by RNA-seq

To evaluate DEG profiles and potential signal regulation, RNA-seq assay was conducted. Transcriptomic analysis obtained approximately

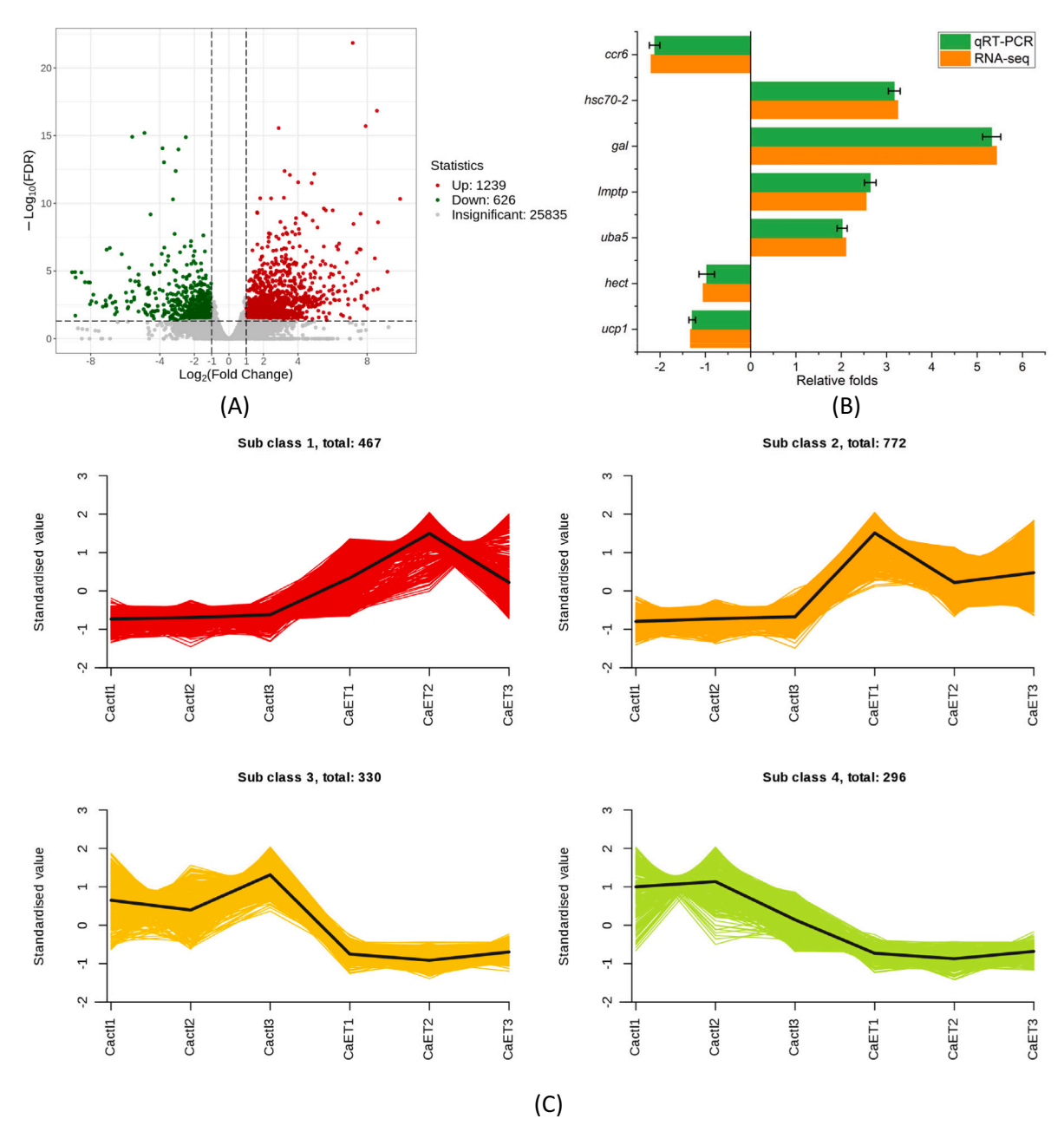


Fig. 2. Characterization of RNA-seq data. (A) DEGs presented by volcano plot. Green spots represented decreased DEGs, while red spots represented increased DEGs. (B) Validation of RNA-seq data by qRT-PCR assay. The calculated data (mean \pm SD) with different letters were significantly different (P < 0.05). (C) Expression patterns of DEGs calculated by K-means clustering analysis. Different expression patterns in four subclasses were labeled with red, orange, yellow and green, respectively.

average 8.60 and 8.05 of clean base (G) from Cactl group and CaET group with $\rm Q_{30}$ values higher than 93.01 % and 93.36 %, respectively. Additionally, GC contents of Cactl group and CaET group were about 47.37 % to 47.87 % and 47.34 % to 47.58 %, respectively. A clear separation of transcriptional features of Cactl group and CaET group was determined by PCA analysis (Fig. S3). A total of 1865 DEGs were obtained in RNA-seq, including 1239 increased DEGs and 626 decreased DEGs (Fig. 2A). In Fig. 2B, seven DEGs (*uba5*, *lmptp*, *gal*, *hsc70-2*, *ucp1*, *hect* and ccr6) were selected for expression validation of transcriptomic results. Then, the similarities of DEG expression patterns were calculated by K-means clustering analysis. In Fig. 2C, four subclasses of DEG profiles were detected in liver of crucian carp after *E. tarda* infection, while the highest DEG number was observed in subclass 2.

GO analysis discovered that "cellular process" enriched the most

DEG numbers (621, 33.30 %) in biological process (BP), possessing 445 increased DEGs and 176 decreased DEGs. "Cellular anatomical entity" was predominant subgroup (755, 40.48 %) in cellular component (CC), containing 519 increased DEGs and 236 decreased DEGs. The major subgroup of transcript was represented by "binding" (592, 31.74 %) in molecular function (MF), possessing 406 increased DEGs and 186 decreased DEGs (Fig. S4A—B). "Purine-containing compound metabolic process" (50, 14.20 %) was the most predominant subclass in TOP50 GO terms, followed by "purine nucleotide metabolic process" (48, 14.37 %), "ribonucleotide metabolic process" (48, 13.64 %) and "ribose phosphate metabolic process" (48, 13.37 %) (Fig. S4C). DEGs were classified into 6 KEGG subcategories (Fig. 3A). "Metabolic pathway" contained the most numbers of DEGs (270, 6.15 %) in the subcategory of "metabolism", while the highest proportion of enriched DEGs was observed in "citrate

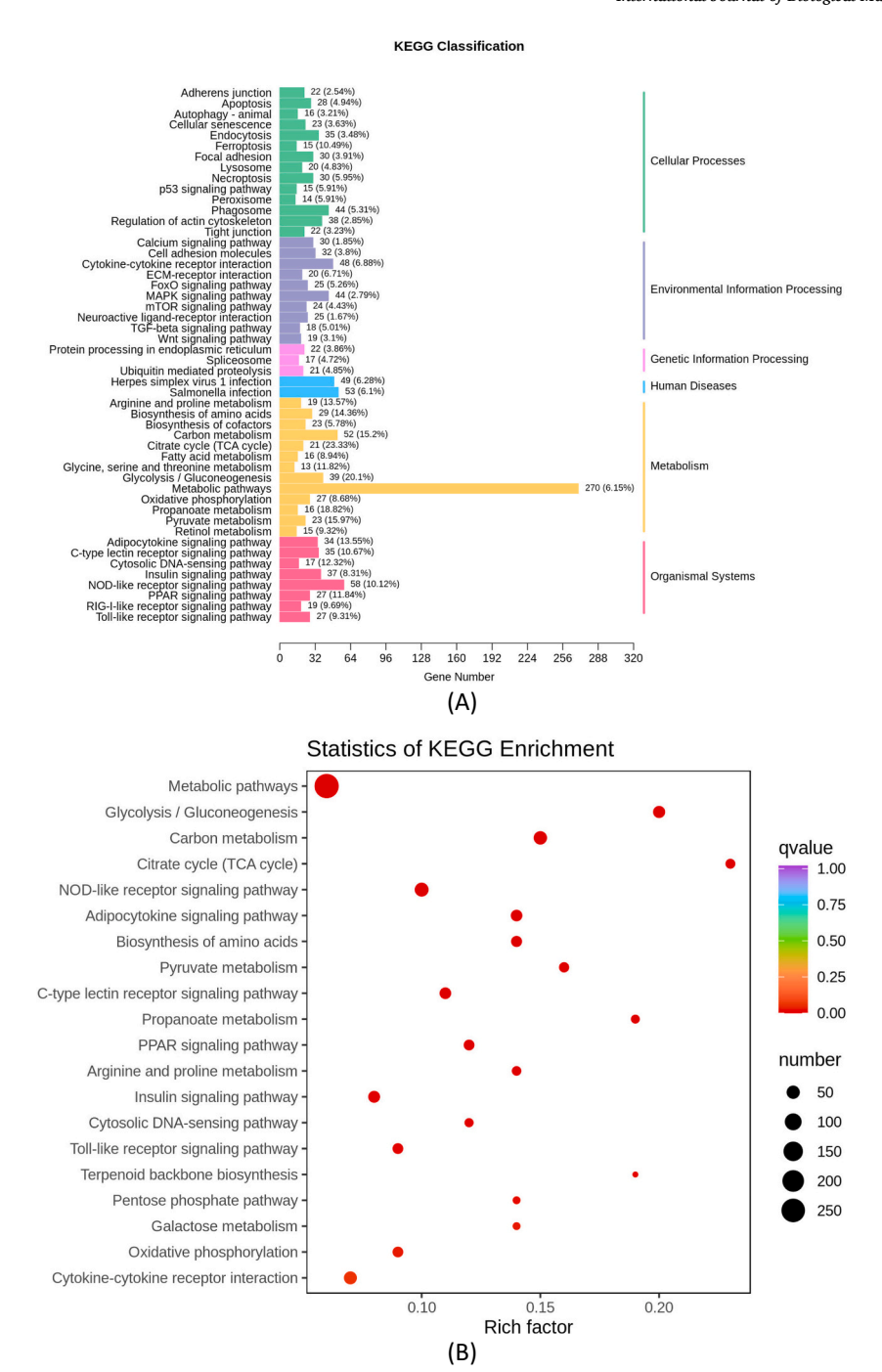


Fig. 3. DEGs statistics by KEGG analysis. (A) Gene proportion calculated by KEGG classification. The subclasses, including cellular processes, environmental information processing, genetic information processing, human diseases, metabolism and organismal systems, were labeled from green to dark pink. (B) DEGs analyzed by Top 20 KEGG enrichment. Sizes of circles represented the numbers of enriched DEGs. Significant difference was distinguished from blue to red.

cycle" (21, 23.33 %) (Fig. 3B).

3.3. Liver metabolic features determined by LC-MS/MS

To characterize crucial metabolic biomarkers in liver of crucian carp after *E. tarda* infection, a total of 3224 metabolites were obtained by LC-MS/MS technology. "Amino acid and its metabolites" presented the highest proportion (17.99 %) among all metabolic classes, followed by "benzene and substituted derivatives" (16.25 %), "heterocyclic compounds" (12.59 %) and "organic acid and its derivatives" (11.63 %) (Fig. 4A). Ile-Trp showed the highest content among all obtained metabolites, followed by tetrahydrocortisone and galactaric acid, while

9,10-EpOME was found to be the metabolite with the lowest content (Fig. 4B). The clear separations of metabolic features were subjected to PLS—DA and OPLS-DA models (Fig. S5A-D). According to OPLS-DA model, S plot analysis was conducted to confirm DM differentiation by calculation of VIP threshold (Fig. S5E). In Fig. 5A, a total of 149 DMs were identified from 1700 secondary metabolites in liver of crucian carp after *E. tarda* challenge, possessing 72 increased metabolites and 77 decreased metabolites. DMs were classified into 20 subclasses by class heatmap analysis. "Amino acid and its metabolites" (29, 19.46 %) contained the most numbers of DMs among subclasses, followed by "organic acid and Its derivatives" (22, 14.77 %) and "benzene and substituted derivatives" (14, 9.40 %) (Fig. 5B-C). Afterwards, relative

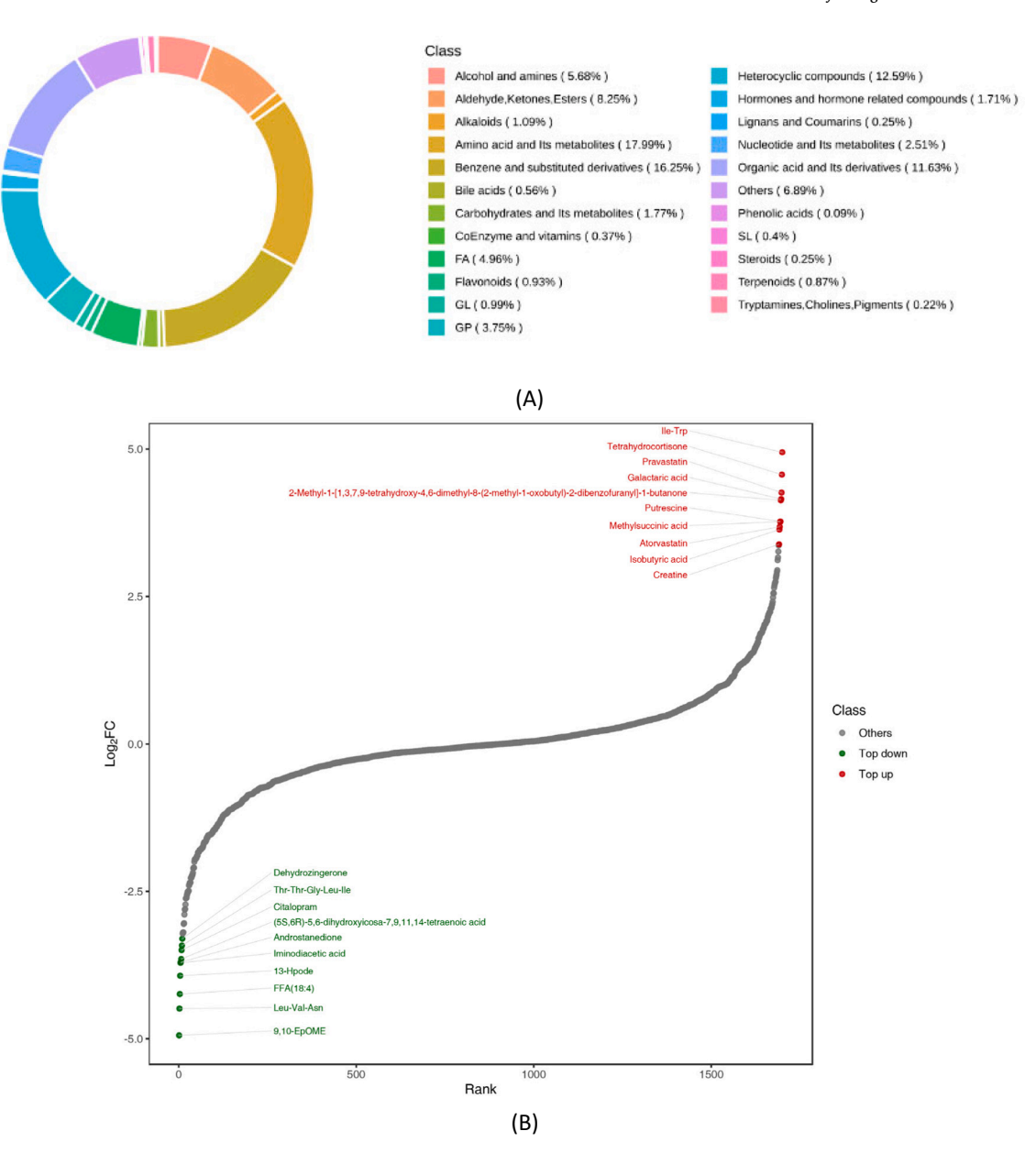


Fig. 4. Metabolic feature in liver of crucian carp following *E. tarda* challenge. (A) Liver metabolic category. Various DMs were classified subclasses labeled from red to dark pink. (B) Dynamic distribution of liver metabolites in crucian carp. DMs with increased Log₂FC values were shown with red labels, while DMs with decreased Log₂FC values were shown with green labels.

contents of TOP50 VIP DMs were measured by Z-score plot. In Fig. S6A, Z-score analysis revealed that most TOP50 VIP DMs increased dramatically in liver of crucian carp after E. tarda infection. "Amino acid and its metabolites" and "organic acid and its derivatives" possessed most numbers of negative-correlated DMs among TOP50 VIP DMs, while most percentages of DMs in "aldehyde, ketones, esters" show a positive correlation with other DMs (Fig. S6B). In addition, spaglumic acid showed the highest VIP score among obtained DMs, followed by followed by pyruvaldehyde and isobutyric acid (Fig. S6C). In Fig. 5D, tetrahydrocortisone showed the highest Log₂FC value among TOP20 VIP DMs, followed by methylsuccinic acid and putrescine, while the lowest DM content was found in Leu-Val-Asn. Afterwards, nine crucial metabolic genes were selected for expression validation (Fig. 5E). Relative expressions of coq10b, acc, prmt1, pemt, odc1 and ApoD were approximately 1.70-, 3.85-, 1.62-, 2.01-, 5.24- and 3.56- fold higher in CaET group by comparing with that of Cactl group, while a sharp decrease of map2b, gamt and dgat2 was observed (p < 0.05).

DMs were classified into 4 KEGG subclasses, while most DMs were enriched in "metabolic pathways" (44, 84.62 %), followed by "biosynthesis of cofactors" (8, 15.38 %), "purine metabolism" (8, 15.38 %) and "nucleotide metabolism" (6, 11.54 %) (Fig. 6A). In Fig. 6B, "purine metabolism" enriched the most numbers of DEGs among Top20 KEGG pathway, while annotated DMs in "regulation of actin cytoskeleton" displayed the highest tendency towards upregulation. Then, relative contents of crucial DMs were further analyzed in three dominant KEGG pathways, including "purine metabolism", "nucleotide metabolism" and "neuroactive ligand-receptor interaction". KEGG analyses revealed that most numbers of DMs in above three KEGG pathways belonged to "nucleotide and its metabolites" and "heterocyclic compounds" (Fig. S7A-C).

3.4. Integrated analysis of multiomics data

All DEGs and DMs were separated by O2PLS model (Fig. 7A-B).

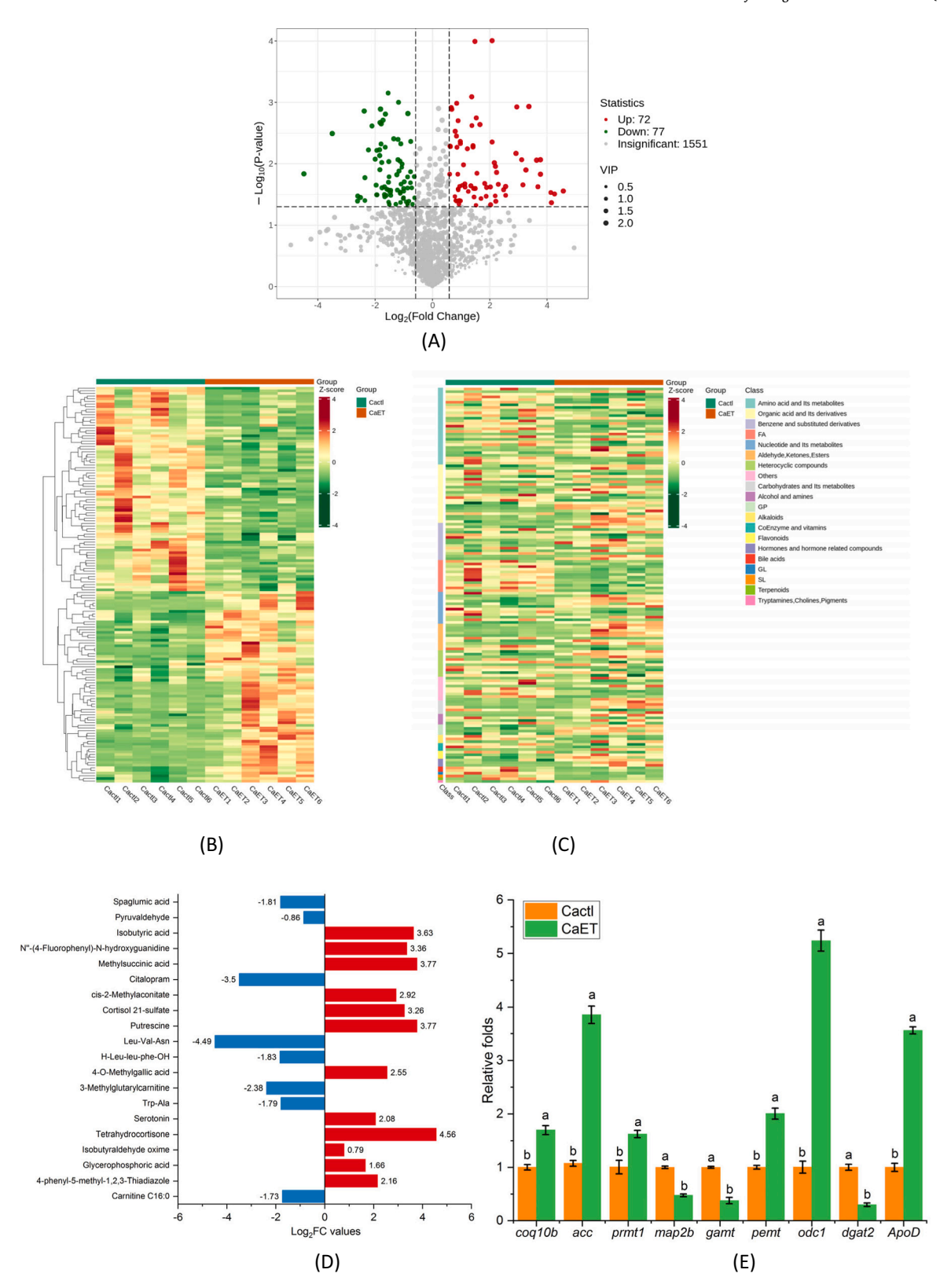


Fig. 5. Characterization of metabolic features. (A) Numbers of increased and decreased DMs by volcano plot. Green spots represented decreased DMs, while red spots represented increased DMs. (B—C) Cluster heatmap and class heatmap analysis of DMs. Increased DMs were labeled with red, while decreased DMs were labeled with green. (D) Validation of metabolic gene expressions by qRT-PCR assay. The calculated data (mean \pm SD) with different letters were significantly different (P < 0.05). (E) Log₂FC values of TOP20 VIP DMs. DMs with increased Log₂FC values were shown with red labels, while DMs with decreased Log₂FC values were shown with blue labels.

KEGG Classification

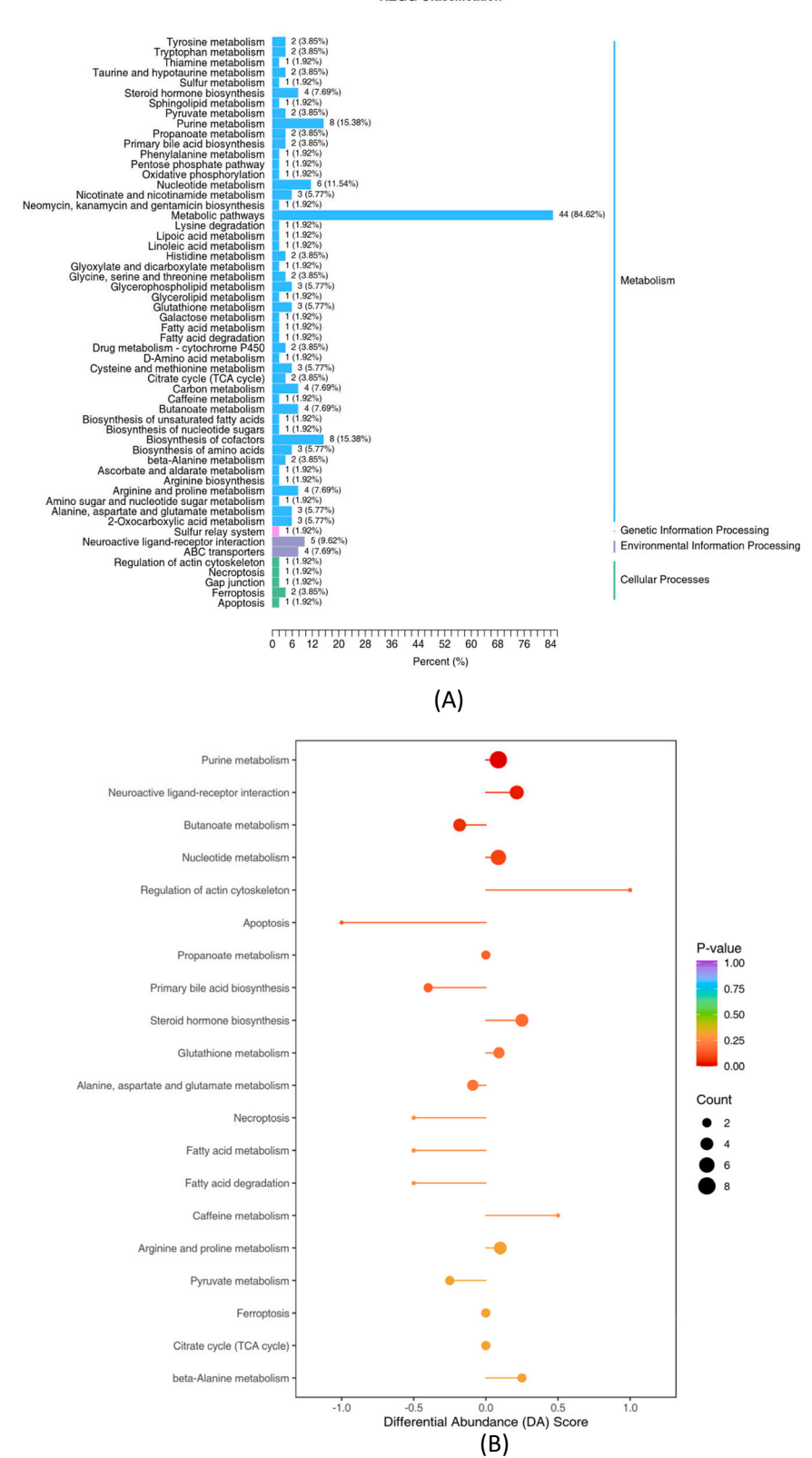


Fig. 6. Signal pathways of DMs in liver following *E. tarda* challenge. (A) KEGG classification of annotated DMs. The subclasses, including metabolism, genetic information processing, environmental information processing and cellular processes, were labeled from blue to green. (B) KEGG pathways of annotated DMs with the calculation of differential abundance (DA) score. The enriched DMs were labeled from red to blue based on *p*-value.

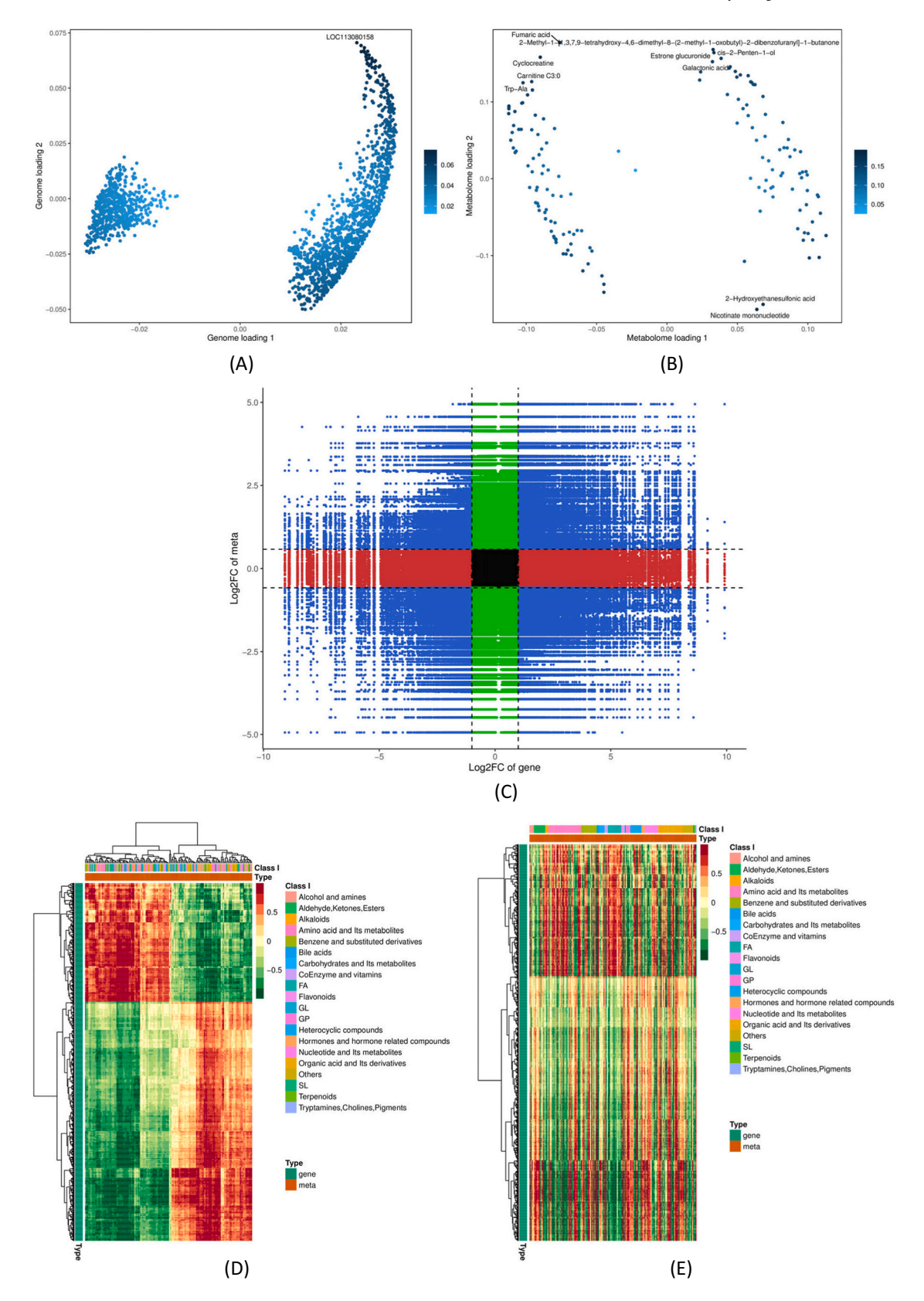


Fig. 7. Integrated analysis of RNA-seq and LC-MS/MS. (A-B) DEGs and DMs were analyzed by O2PLS models. (C) Co-expression patterns of DEGs and DMs were analyzed by nine quadrant plots. Genes and metabolites without differential expression were presented in the fifth quadrant. Co-expression patterns of DEGs and DMs showing positive correlation were presented in the third and seventh quadrant. Co-expression patterns of DEGs and DMs showing negative correlation were presented in the first and ninth quadrant. Co-expression patterns of DEGs and DMs possessing no correlations were presented in the second, fourth, sixth and eighth quadrant. (D-E) Correlation heatmap analysis of DEGs and DMs. Positive correlations of DEGs and DMs were labeled with red, while negative correlations of DEGs and DMs were labeled with green.

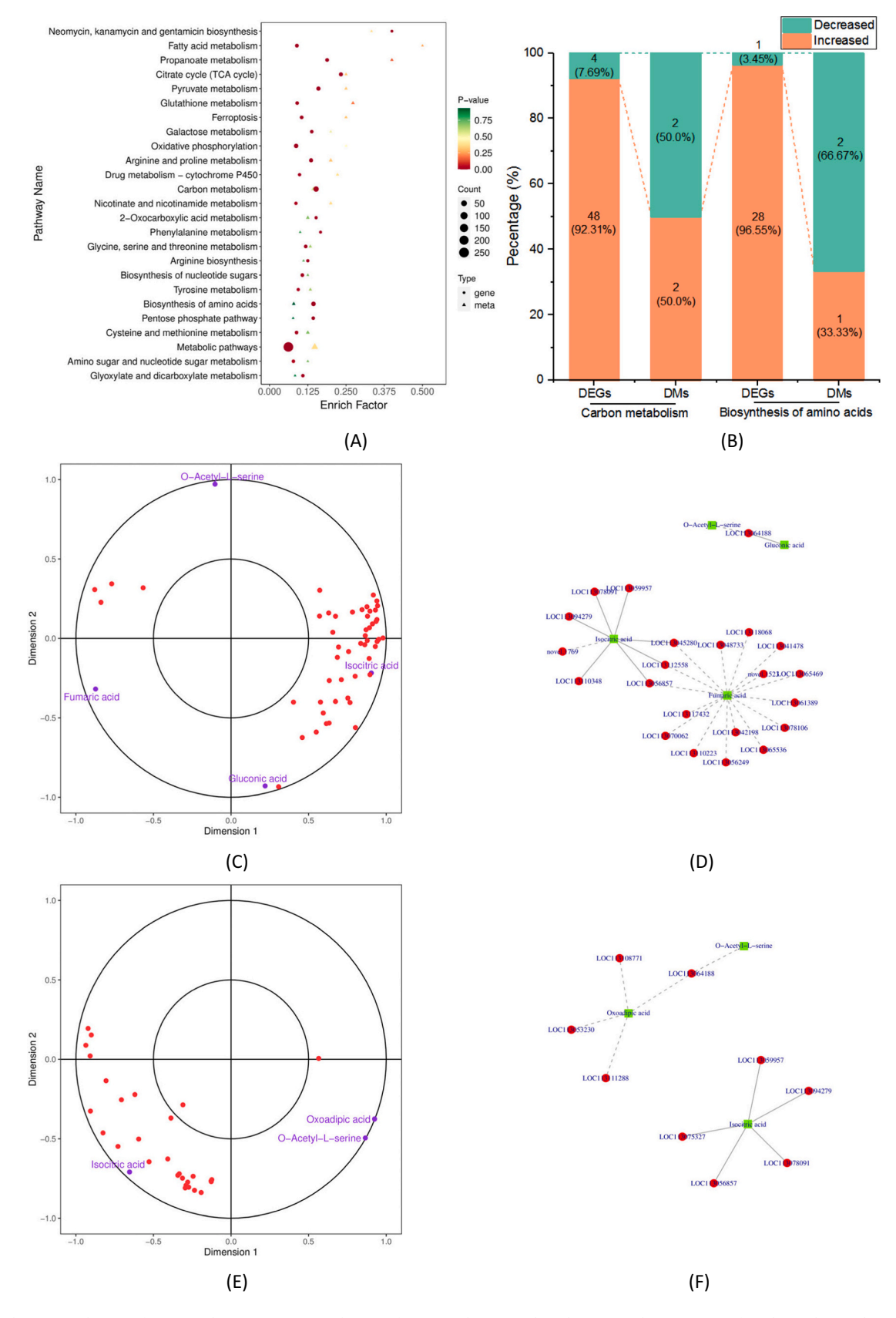


Fig. 8. Shared KEGG pathways of DEGs and DMs. (A) Co-enrichment of DEGs and DMs in shared KEGG pathways. Sizes of circles and triangles represented the enriched numbers of DEGs and DMs, respectively. Significant differences were distinguished from green to red. (B) Percentages of DEGs and DMs in "Carbon metabolism" and "Biosynthesis of amino acids". (C-D) The correlation of DEGs and DMs in "Carbon metabolism". (E-F) The correlation of DEGs and DMs in "Biosynthesis of amino acids".

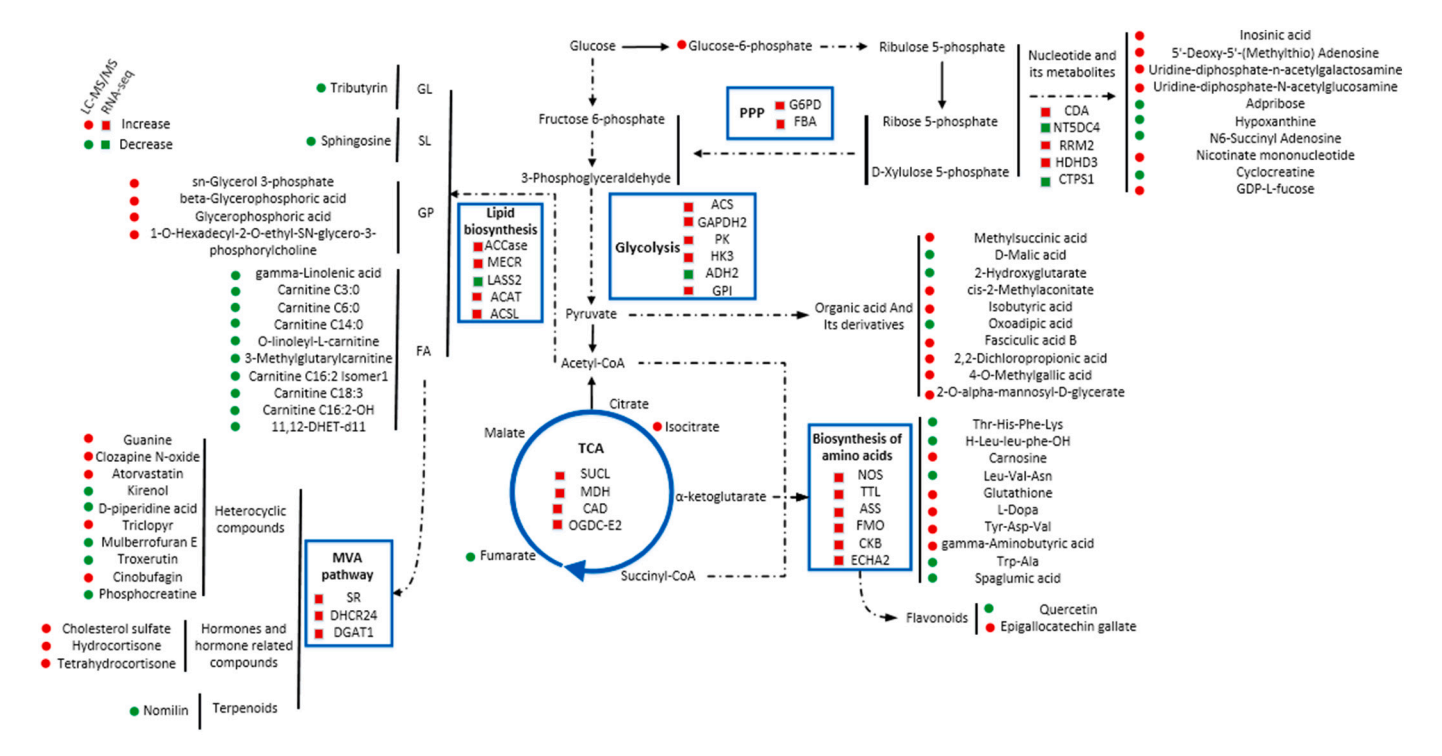


Fig. 9. Interactive network analysis of DEGs and DMs in liver of crucian carp following *E. tarda* challenge. DEGs and DMs were indicated by squares and circles, respectively.

Afterwards, positive correlation of DEGs and DMs were shown in the third quadrant (20.40 %) and the seventh quadrant (29.92 %) by nine quadrant analysis, while negative correlation of DEGs and DMs were presented in the first quadrant (16.57 %) and the ninth quadrant (33.11 %) (Fig. 7C). Correlation heatmap analysis revealed that positive- or negative-correlated DMs and DEGs may predominantly belong to 3 subclasses of metaboltes, including "amino acid and its metabolites" (22.91 %), "organic acid and its derivatives" (16.35 %) and "benzene and substituted derivatives" (9.99 %) (Fig. 7D-E).

In Fig. S8, integrated analysis of DEGs and DMs revealed that a total of 776 DEGs and 52 DMs were mapped to 25 shared KEGG pathways. Among them, "metabolic pathways" enriched the most numbers of DEGs and DMs, followed by "carbon metabolism" and "biosynthesis of amino acids" (Fig. 8A). "Carbon metabolism" possessed 48 increased DEGs and 4 decreased DEGs, along with 2 increase DMs (gluconic acid and isocitric acid) and 2 decreased DMs (fumaric acid and O-Acetyl-L-serine). In contrast, "biosynthesis of amino acids" contained 28 increased DEGs and 1 decreased DEGs, along with 1 increased DM (isocitric acid) and 2 decreased DMs (O-Acetyl-L-serine and oxoadipic acid) (Fig. 8B). Canonical correlation analysis (CCA) revealed that isocitric acid showed the closest correlation with DEGs. In addition, isocitric acid showed the positive correlation with DEGs than other DMs, while fumaric acid and oxoadipic acid were negative-correlated with most DEGs in "carbon metabolism" and "biosynthesis of amino acids", respectively (Fig. 8C-F).

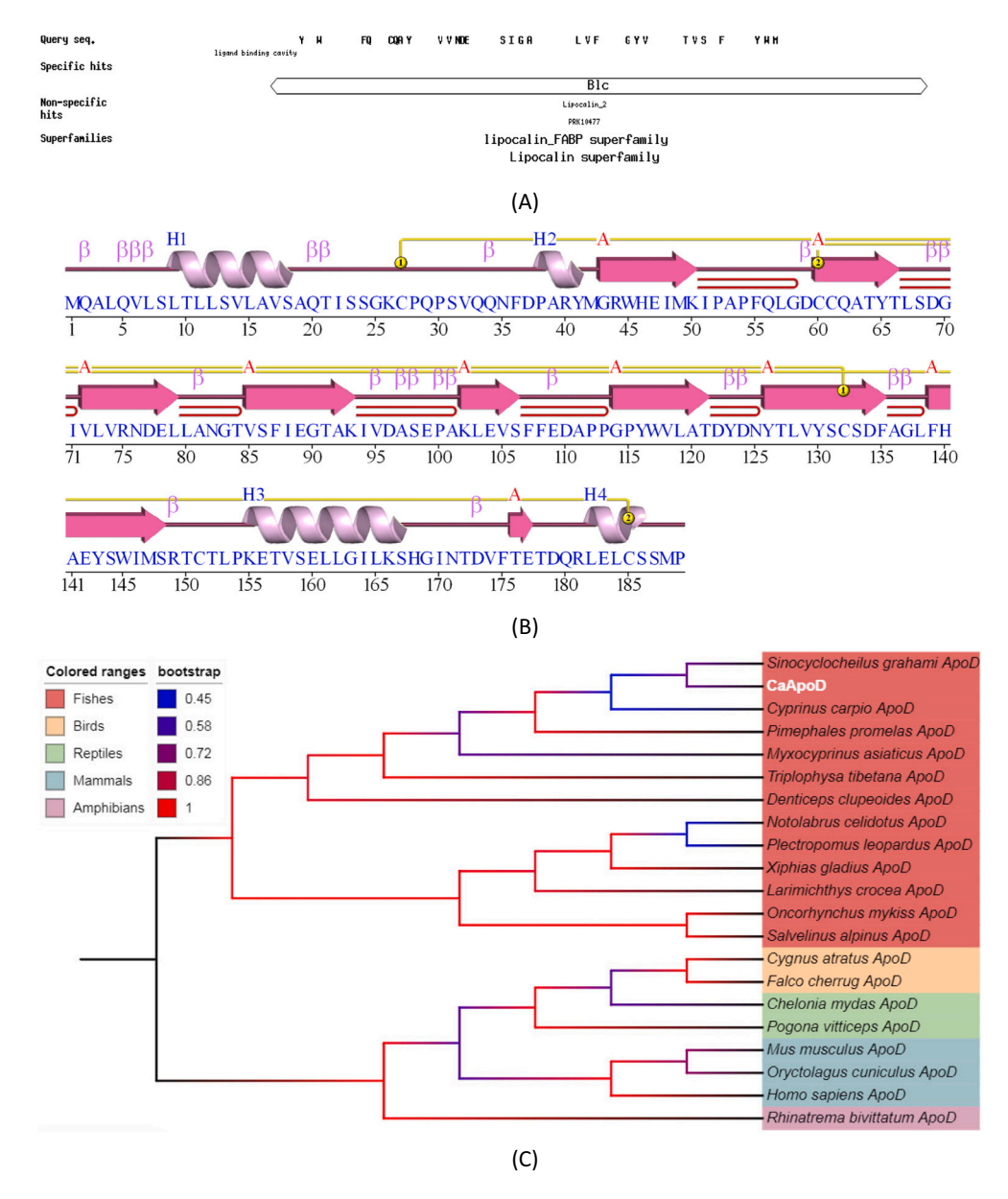
To further investigate the comprehensive interplay of all crucial DMs (p-value <0.05, TOP10 VIP in pathways) and DEGs (p-value <0.05, $|\log_2 FC| \geq 1$), pathway network was shown in Fig. 9. Expression profiles of indicator genes significantly altered in pentose phosphate pathway (PPP), glycolysis, tricarboxylic acid (TCA) cycle, lipid biosynthesis, mevalonic acid (MVA) pathway and amino acid metabolism. In contrast, the detected numbers of TOP10 VIP DMs in metabolic intermediates of lipids, organic acids, nucleotides and amino acids were higher than that of glycolysis and TCA cycle.

3.5. Sequence identification and gene expression of CaApoD

The ORF sequence of *CaApoD* was extracted from above omics data, which encoded a polypeptide of 189 amino acid residues with an estimated molecular mass of 20.84 kDa and a predicted isoelectronic point of 4.37. In Fig. 10A, a high-conserved signal peptide $(M^1Q^2A^3L^4Q^5V^6L^7S^8L^9T^{10}L^{11}L^{12}S^{13}V^{14}L^{15}A^{16}V^{17}S^{18}),$ a lipocalin_apoD-like domain and 27 ligand binding cavities were found in the structure of CaApoD. In Fig. 10B, secondary structure of CaApoD contained 5 β -bulges, 7 β -hairpins, 9 strains, 4 helices, 23 β -turns, 2 disulfide bonds and 1 sheet. In Fig. 10C, phylogenetic tree analysis suggested that CaApoD amino acid sequence showed a higher similarity to the counterparts of other freshwater teleosts.

Ramachandran plot analysis revealed that 89.2 % of amino acid residues in the deduced CaApoD structure belonged to "most favored regions" and 8.40 % of amino acid residues were "additional allowed regions" (Fig. 11A). In Fig. 11B-C, tertiary structure of CaApoD showed a close identity to c2hzqA template modeled with exceeding a 90 % confidence, possessing 4 cavities, 1 interior cavities and 2 tunnels. In Fig. 11D, tertiary structure of CaApoD also contained 2 predominant binding sites in active clefts with the largest volumes of 5083.17 A^3 (marked in red) and 2279.39 A^3 (marked in purple), respectively. In addition, 1 pore was found in the tertiary structure of CaApoD with the length of 31.10 Å (Fig. 11E).

In Fig. 12A, the highest level of CaApoD expression was observed in liver, followed by kidney, spleen and gill, while its expression showed the lowest level in muscle (p < 0.05). In Fig. 12B, CaApoD expression markedly increased from 12 h to 24 h and attained the peaked levels in liver at 24 h after A. hydrophila challenge, followed by a gradual decline from 24 h to 48 h (p < 0.05). In Fig. 12C, crucian carp infected with A. hydrophila exerted increased profiles of CaApoD expressions in kidney with the peaked level at 48 h (p < 0.05). In Fig. 12D, splenic CaApoD expression began to increase at 12 h and peaked at 24 h after A. hydrophila infection, followed by a sharp decrease from 24 h to 48 h (p < 0.05).



3.6. Inhibitory effect of CaApoD fusion protein on fish pathogens

In Fig. 13A, a strong fusion protein band was observed in whole cell lysate of pET32a-CaApoD transformed cells after IPTG induction in comparison with that of the control. Then, purified CaApoD fusion protein was confirmed by western blotting. Afterwards, *in vitro* effect of CaApoD fusion protein on growth rate and biofilm formation of fish pathogens were evaluated. The treatment of CaApoD can obviously reduce the biofilm formation ability of *E. tarda* and *A. hydrophila* to 63.22 % and 52.76 % by comparing with that of pET32a tag group (p < 0.05) (Fig. 13B). In Fig. 13C-D, binding index towards *A. hydrophila* and *E. tarda* gradually increased in CaApoD group by comparing with that of pET32a tag group, when the protein concentration increased (p < 0.05).

In addition, CaApoD treatment could dramatically decrease the growth rates of *A. hydrophila* or *E. tarda* in comparison with that of pET32a tag group (p < 0.05) (Fig. 13E-F).

4. Discussion

E. tarda is the major etiologic agent of edwardsiellosis characterized by infectious symptoms of ascites, hernia, exophthalmia and organic lesions [28]. Since *E. tarda* is an intracellular pathogen that cannot be effectively restricted by most antibiotics administration, it poses an increasing threat to the health of freshwater and marine farmed fish [10]. In this study, increased expression of *mukf* gene was observed in isolated tissues of crucian carp following *E. tarda* challenge, along with

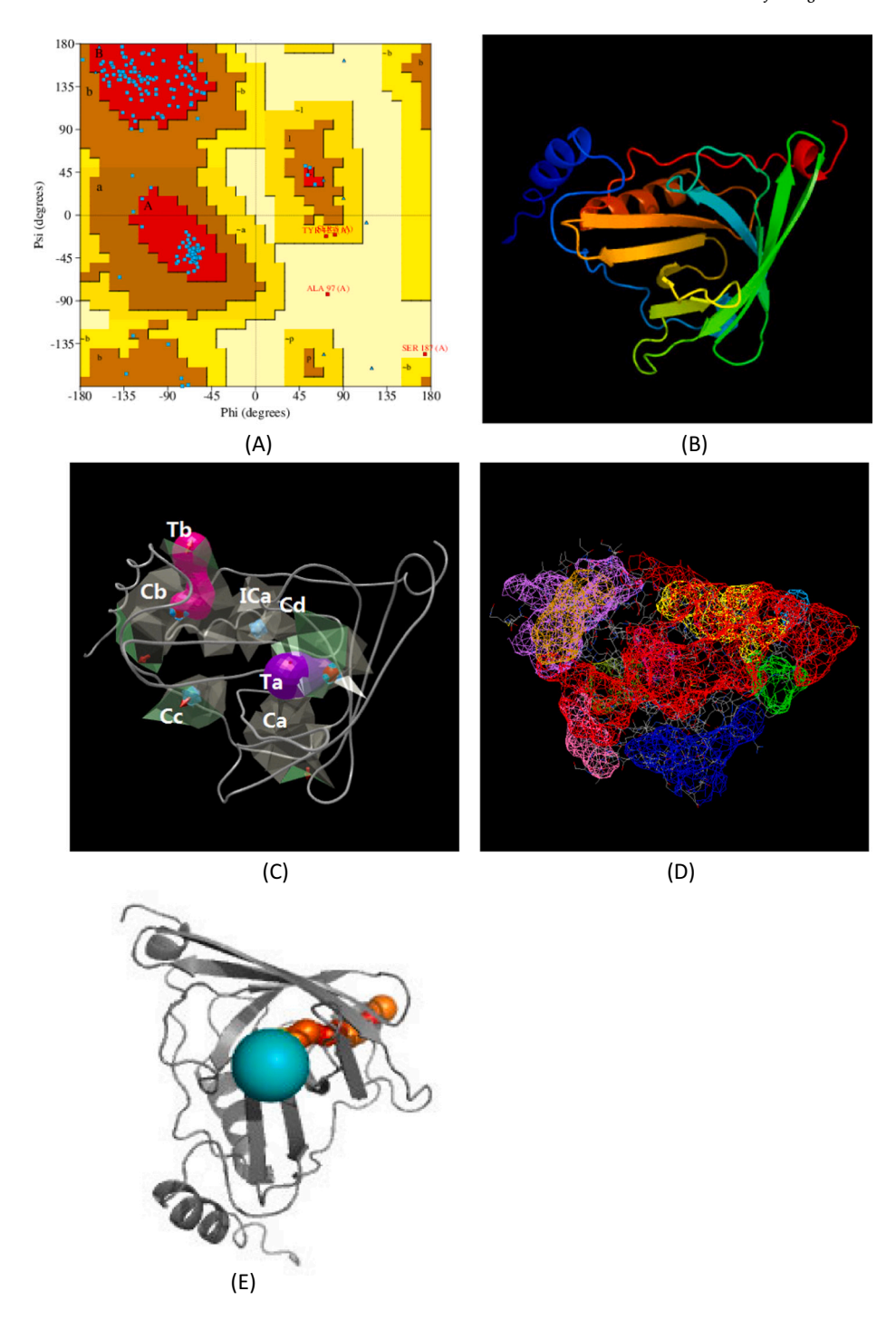


Fig. 11. Tertiary structure of CaApoD. (A) Ramachandran plot analysis of CaApoD structure. (B) The deduced tertiary structure of CaApoD. Structures were colored by rainbow from N to C terminus. (C) Crucial domains in tertiary structure of CaApoD. Cavity was labeled by Ca, Cb...; Interior cavity was labeled by Ica; Tunnel was labeled by Ta and Tb. (D) Binding sites at active cleft domains in tertiary structure of CaApoD. Binding sites were colored by rainbow. (E) Pore structure predicted in tertiary structure of CaApoD.

increased levels of liver injury. Liver enzymatic activities of CAT, GR, SDH and LDH decreased sharply in crucian carp following *E. tarda* challenge, while AKP and AST activity increased significantly. In general, redox-related enzymes, such as CAT, GR, SDH and LDH, are widely considered as pivotal indicators that play the regulatory roles in antioxidant function of teleost fish under the exposure to various stressors [29], whereas AKP and AST were the crucial disease-related enzymes related to injury status of fish organs [30]. Moreover, endogenous antioxidants and antioxidant enzymes can eliminate free radicals and alleviate cytokine-induced cytotoxicity [31], but long-term induction of

oxidative stress may suppress antioxidant response within the host, which may further play a detrimental role in immunometabolic processes [32]. These results suggested that *E. tarda* infection may lead to the collapse of antioxidant defense in liver, along with increased levels of metabolic pathology. However, the global understanding of pathological response in *E. tarda*-infected crucian carp remains unclear.

In order to explore the immunometabolic interplay in crucian carp after *E. tarda* infection, transcriptome and metabolome were implemented. In this investigation, most DEGs were predominantly enriched in metabolic pathways, such as carbohydrate metabolism, amino acid

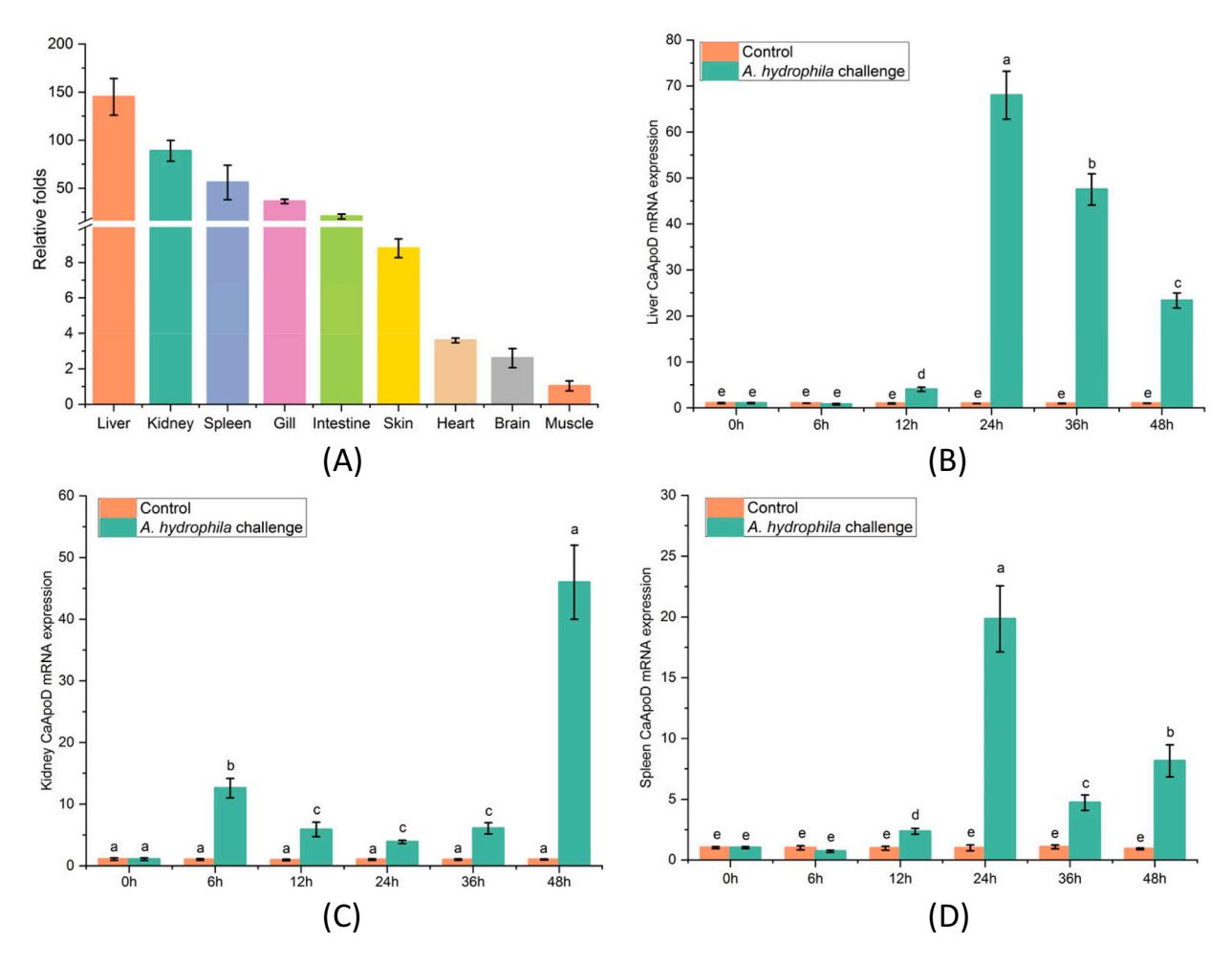


Fig. 12. Expression patterns of CaApoD. (A) Tissue-specific expressions detected by qRT-PCR assay. (B-D) Expressions of CaApoD were detected in liver, kidney and spleen at 0, 6, 12, 24, 36 and 48 h post-challenge. The calculated data (mean \pm SD) with different letters were significantly different (P < 0.05) among the groups.

biosynthesis, adipocytokine signal pathway and PPAR signal pathway, and immune related pathways, such as NOD-like receptor (NLR) signal pathway, Toll-like receptor (TLR) signal pathway and C-type lectin receptor (CLR) signal pathway, whereas DMs were mainly enriched in amino acids and organic acids. In general, liver is one of pivotal organs that can participate in immune regulation, detoxication and nutritional metabolism [33]. These results indicated that E. tarda infection could dramatically alter immune regulation and metabolic processes in liver of crucian carp. Afterwards, multiomics analyses revealed that a total of 776 DEGs and 52 DMs were mapped to 25 shared KEGG pathways, while carbohydrate and amino acid metabolism appeared to play important roles in immunometabolic regulation in liver of E. tarda-infected crucian carp. Among detected DMs, spaglumic acid should be identified as one of crucial liver biomarkers with the highest VIP score, while tetrahydrocortisone showed the highest Log₂FC value among TOP20 VIP DMs. In addition, isocitric acid showed the closest correlation with DEGs of carbon metabolism and amino acid metabolism in liver of crucian carp following E. tarda infection. Generally speaking, metabolic processes of carbohydrates may not only supply energy for individual development, but also mediate immune and physiological response upon infection [34,35]. Metabolic intermediates of TCA cycle can participate in immune cell activation and cytokine production [36,37]. Previous studies indicated that isocitric acid was an important intermediate of TCA cycle that could show a positive correlation with liver diseases [38]. Fatty acids, another important energy sources, can also influence antigen presentation and immune cell response [39]. Mevalonic acid is a unique fatty acid intermediate that can determine the steroid biosynthesis [40]. Recent study indicates that steroid hormones are involved in production of AMPs [41] and alleviate pathological status during pathogenic infection [42]. Tetrahydrocortisone is one of important steroid derivatives, which was widely considered as one of metabolic biomarkers in teleost fish exposed to in vitro stimuli [20]. Amino acids serve as preferential energy sources together with lipids [43], but its short supply may cause the impairment of immune function, which may increase host susceptibility to invading pathogens [44]. Spaglumic acid serves as an agonist of N-methyl-D-aspartate (NMDA) and glutamate receptor, which can participate in a wide range of immunological response [45]. Recent findings demonstrate that active NMDA glutamate receptor can participate in cytokine production in lymphocytes via regulation of NF-κB and c-Fos [46] and modulate the release of glutamate in neutrophils [47]. Thus, taken together, E. tarda challenge aggravated oxidative stress-induced tissue damage and affected the metabolic processes of carbohydrates and amino acids in crucian carp.

In general, AMPs belong to a group of LWC peptides that play important roles in immune defense against invading pathogens [48]. As is well known, AMPs are biological macromolecules produced in different cell types that can restrict bacterial growth by directly forming pores in membranes, which is largely due to their signature sequences, including amino acid composition, amphipathicity, cationic charge and molecular weight [17]. Recently, omics research may further provide a systematic insight into confirmation of AMP genes according to common features and species-specific characteristics among various fish species [49]. In this study, several hub genes involved in immunometabolic

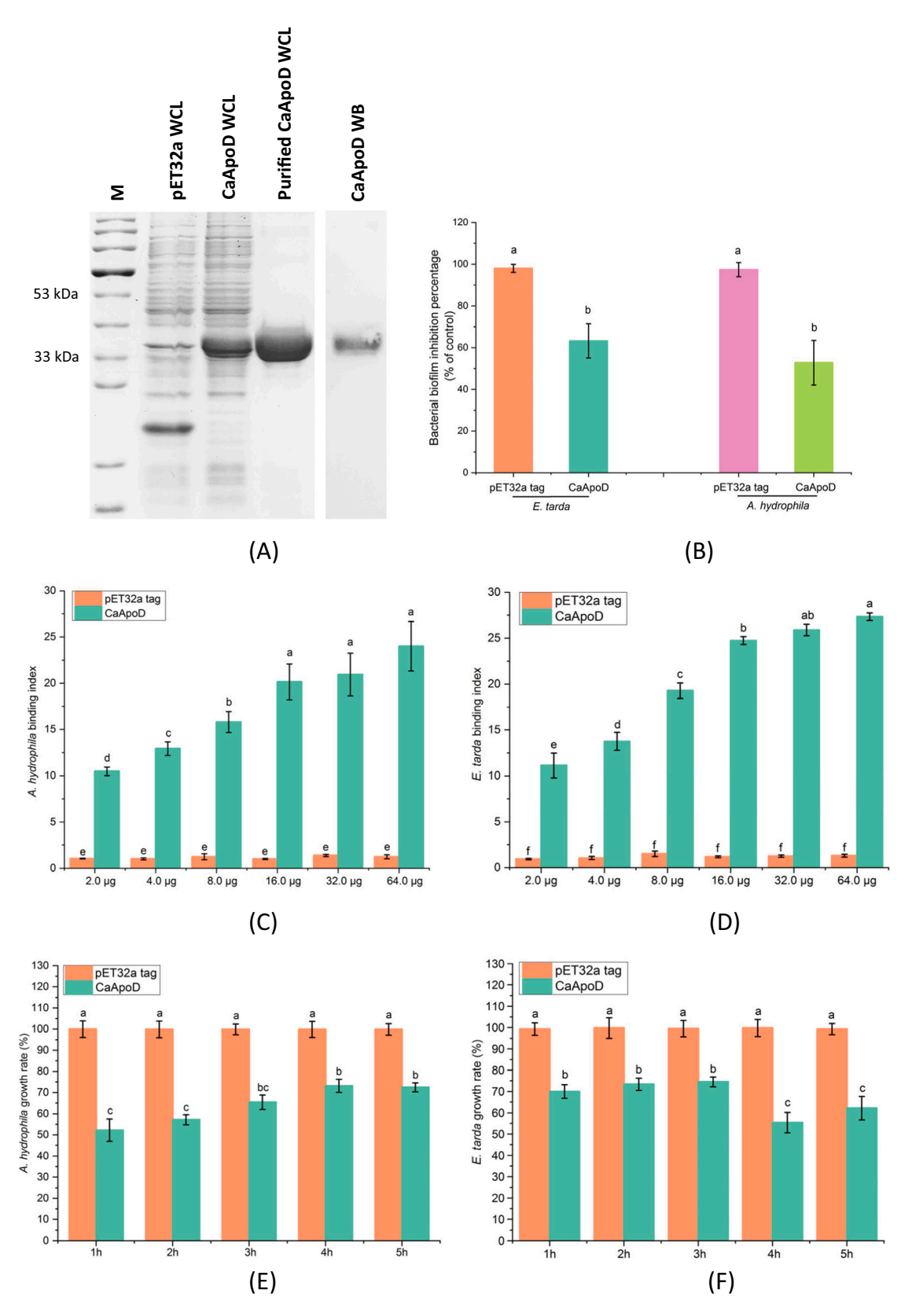


Fig. 13. Production and antimicrobial activity of CaApoD. (A) Production and validation of CaApoD fusion protein. Lane M: protein molecular standard; Lane pET32 α WCL: total protein was isolated from lysate of pET32 α -BL21 after IPTG induction; Lane CaApoD WCL: total protein was isolated from lysate of pET32 α -CaApoD-BL21 after IPTG induction; Lane purified CaApoD WCL: CaApoD fusion protein was purified by using Ni-NTA resin; Lane CaApoD WB: purified CaApoD fusion protein was identified by using anti-His tag antibody. (B) Inhibition of biofilm forming activity of *A. hydrophila* and *E. tarda* by the administration of CaApoD. (C-D) Bacterial binding activity of ApoD fusion protein to *A. hydrophila* and *E. tarda*. (E-F) Effect of ApoD fusion protein on growth rates of *A. hydrophila* and *E. tarda*. The calculated data (mean \pm SD) with different letters were significantly different (P < 0.05) among the groups.

regulation were selected for validation of gene expressions. Expression levels of uba5, lmptp, gal, hsc70-2, coq10b, acc, prmt1, pemt, odc1 and ApoD increased markedly in liver of crucian carp after E. tarda infection, while decreased expressions of ucp1, hect, ccr6, map2b, gamt and dgat2 were observed. Among hub genes, ApoD encoding an atypical apolipoprotein not only confers protection against oxidative stress [50], but also acts as a pathological marker of severe diseases in human, including dyslipidemia, atherosclerosis, breast cancer and Alzheimer's disease [51,52]. In addition, *ApoD* sequence was firstly identified as one of novel AMP genes from fish transcriptome by utilizing high-conserved regions in AMPs of other teleosts [53]. Although sequence prediction has been conducted, there is a lack of evidence that fish apoD contributes to the antimicrobial function. Therefore, ApoD gene was identified as one of hub genes from above omics data showing an increased expression, which was selected for further study. CaApoD sequence encoded 3 highly conserved motifs: a signal peptide, a lipocalin apoD-like domain and 27 ligand binding cavities. Expression analysis by qRT-PCR assay indicated that CaApoD expression was broadly observed in isolated tissues with the highest expression in liver. Then, the expression profiles of CaApoD mRNA were investigated in immune-related tissues upon A. hydrophila challenge. Liver, kidney and spleen are major immunerelated organs in fish, playing pivotal roles in immune defense against invading pathogens [54]. In current finding, the increased profiles of CaApoD expressions were observed in liver, kidney and spleen upon infection. These results suggested that CaApoD belonging to the members of apolipoprotein family may respond to the bacterial infection. To further evaluate the inhibitory effect on fish pathogens, CaApoD fusion protein was produced in vitro. In this investigation, ELISA assay revealed that CaApoD could directly bind to A. hydrophila and E. tarda in a dosedependent manner. Following that, treatment of CaApoD fusion protein could dramatically decrease ratios of biofilm formation and growth performance of A. hydrophila and E. tarda. Thus, taken together, we predicted that CaApoD could exhibit the suppressive role in bacterial growth rates and biofilm forming activities by directly binding to the cell wall of A. hydrophila and E. tarda.

In summary, we characterized antioxidant status and pathological features in liver of crucian carp following E. tarda challenge. A core set of hub metabolites and key genes involved in immune modulation and metabolic homeostasis were identified by multiomics analyses. Spaglumic acid, isocitric acid and tetrahydrocortisone were considered as the crucial liver biomarkers in E. tarda-infected crucian carp. In addition, carbon and amino acid metabolism may play the predominant role in liver metabolism. After that, CaApoD sequence was identified from multiomics data of E. tarda-infected crucian carp. We characterized CaApoD architecture and studied its expression patterns in healthy crucian carp and E. tarda-infected crucian carp, respectively. Moreover, we confirmed that CaApoD protein could mediate the in vitro binding to A. hydrophila and E. tarda, attenuate bacterial growth as well as diminish bacterial biofilm forming activity for the first time. Our results highlighted molecular and metabolic characteristics underlying the immunometabolic mechanisms in liver of E. tarda-infected crucian carp and in vitro identification of antimicrobial activity of CaApoD against fish pathogens.

CRediT authorship contribution statement

Fei Wang: Software, Methodology, Investigation, Formal analysis, Data curation. Ning-Xia Xiong: Software, Formal analysis, Data curation, Conceptualization. Jie Ou: Validation, Formal analysis. Zi-Rou Zhong: Validation, Formal analysis. Jin-Fang Huang: Validation, Formal analysis. Ke-Xin Li: Validation, Formal analysis. Ming-Zhu Huang: Conceptualization. Zi-Xuan Fang: Validation. Xu-Ying Kuang: Validation. Zi-Le Qin: Validation, Formal analysis. Sheng-Wei Luo: Writing – review & editing, Writing – original draft, Supervision, Project administration, Funding acquisition, Conceptualization.

Declaration of competing interest

The authors declare that they have no conflict of interest.

Data availability

Data will be made available on request.

Acknowledgements

This research was supported by the National Natural Science Foundation of China, China (grant no. 31902363) and Hunan Provincial Natural Science Foundation of China, China (grant no. 2021JJ40340).

Appendix A. Supplementary data

Supplementary data to this article can be found online at $\frac{https:}{doi.}$ org/10.1016/j.ijbiomac.2024.134898.

References

- [1] Z. Li, Z.W. Wang, Y. Wang, J.F. Gui, Crucian carp and gibel carp culture, in: Aquaculture in China: Success Stories and Modern Trends, 2018, pp. 149–157.
- [2] C.J. Bayne, L. Gerwick, The acute phase response and innate immunity of fish, Dev. Comp. Immunol. 25 (2001) 725–743.
- [3] Q. Bernard, A.A. Smith, X. Yang, J. Koci, S.D. Foor, S.D. Cramer, et al., Plasticity in early immune evasion strategies of a bacterial pathogen, Proc. Natl. Acad. Sci. 115 (2018) E3788–E3797.
- [4] C. Secombes, T. Wang, S. Hong, S. Peddie, M. Crampe, K. Laing, et al., Cytokines and innate immunity of fish, Dev. Comp. Immunol. 25 (2001) 713–723.
- [5] N.C. Bols, J.L. Brubacher, R.C. Ganassin, L.E. Lee, Ecotoxicology and innate immunity in fish, Dev. Comp. Immunol. 25 (2001) 853–873.
- [6] S. Luo, F. Xie, Y. Liu, W.-N. Wang, Molecular cloning, characterization and expression analysis of complement component C8 beta in the orange-spotted grouper (Epinephelus coioides) after the Vibrio alginolyticus challenge, Gene 558 (2015) 291–298.
- [7] R. Wang, R. Tang, B. Li, X. Ma, B. Schnabl, H. Tilg, Gut microbiome, liver immunology, and liver diseases, Cell. Mol. Immunol. 18 (2021) 4–17.
- [8] N.-X. Xiong, F. Wang, W.-S. Luo, J. Ou, Z.-L. Qin, M.-Z. Huang, et al., Tumor necrosis factor α2 (TNFα2) facilitates gut barrier breach by Aeromonas hydrophila and exacerbates liver injury in hybrid fish, Aquaculture 739995 (2023).
- [9] S.-Y. Li, N.-X. Xiong, K.-X. Li, J.-F. Huang, J. Ou, F. Wang, et al., Cloning, expression and functional characterization of recombinant tumor necrosis factor α1 (TNFα1) from white crucian carp in gut immune regulation, Int. J. Biol. Macromol. 254 (2024) 127770.
- [10] T. Xu, X.-H. Zhang, Edwardsiella tarda: an intriguing problem in aquaculture, Aquaculture 431 (2014) 129–135.
- [11] S. Maekawa, P.-C. Wang, S.-C. Chen, Comparative study of immune reaction against bacterial infection from transcriptome analysis, Front. Immunol. 10 (2019) 153.
- [12] J. Yang, D. Wang, Y. Li, H. Wang, Q. Hu, Y. Wang, Metabolomics in viral hepatitis: advances and review, Front. Cell. Infect. Microbiol. 13 (2023) 1189417.
- [13] C. Chen, J. Wang, D. Pan, X. Wang, Y. Xu, J. Yan, et al., Applications of multi-omics analysis in human diseases, MedComm 4 (2023) e315.
- [14] A. Lercher, H. Baazim, A. Bergthaler, Systemic immunometabolism: challenges and opportunities, Immunity 53 (2020) 496–509.
- [15] L.A. O'Neill, R.J. Kishton, J. Rathmell, A guide to immunometabolism for immunologists, Nat. Rev. Immunol. 16 (2016) 553–565.
- [16] R. Rathinakumar, W.F. Walkenhorst, W.C. Wimley, Broad-spectrum antimicrobial peptides by rational combinatorial design and high-throughput screening: the importance of interfacial activity, J. Am. Chem. Soc. 131 (2009) 7609–7617.
- [17] K.A. Brogden, Antimicrobial peptides: pore formers or metabolic inhibitors in bacteria? Nat. Rev. Microbiol. 3 (2005) 238.
- [18] R.E. Hancock, Cationic peptides: effectors in innate immunity and novel antimicrobials, Lancet Infect. Dis. 1 (2001) 156–164.
- [19] J. Ageitos, A. Sánchez-Pérez, P. Calo-Mata, T. Villa, Antimicrobial peptides (AMPs): ancient compounds that represent novel weapons in the fight against bacteria, Biochem. Pharmacol. 133 (2017) 117–138.
- [20] N.-X. Xiong, Z.-W. Mao, J. Ou, L.-F. Fan, Y. Chen, S.-W. Luo, et al., Metabolite features and oxidative response in kidney of red crucian carp (Carassius auratus red var) after Aeromonas hydrophila challenge, Comp. Biochem. Physiol., Part C: Toxicol. Pharmacol. 255 (2022) 109293.
- [21] C.-H. Cheng, Y.-L. Su, H.-L. Ma, Y.-Q. Deng, J. Feng, X.-L. Chen, et al., Effect of nitrite exposure on oxidative stress, DNA damage and apoptosis in mud crab (Scylla paramamosain), Chemosphere 239 (2020) 124668.
- [22] L. Wang, C. Fan, W. Xu, Y. Zhang, Z. Dong, J. Xiang, et al., Characterization and functional analysis of a novel C1q-domain-containing protein in Japanese flounder (Paralichthys olivaceus), Dev. Comp. Immunol. 67 (2017) 322–332.
- [23] C.-H. Cheng, S.-W. Luo, C.-X. Ye, A.-L. Wang, Z.-X. Guo, Identification, characterization and expression analysis of tumor suppressor protein p53 from

- pufferfish (Takifugu obscurus) after the Vibrio alginolyticus challenge, Fish Shellfish Immunol. 59 (2016) 312–322.
- [24] G.-H. Cha, S.-W. Luo, Z.-h. Qi, Y. Liu, W.-N. Wang, Optimal conditions for expressing a complement component 3b functional fragment (a2-macroglobulin receptor) gene from Epinephelus coioides in Pichia pastoris, Protein Expr. Purif. 109 (2015) 23–28.
- [25] S.-W. Luo, K.-K. Luo, S.-J. Liu, ITLN in diploid hybrid fish (Carassius auratus cuvieri

 QX Carassius auratus red var

 g) is involved in host defense against bacterial infection, Dev. Comp. Immunol. 103 (2020) 103520.
- [26] C. De La Fuente-Núñez, V. Korolik, M. Bains, U. Nguyen, E.B. Breidenstein, S. Horsman, et al., Inhibition of bacterial biofilm formation and swarming motility by a small synthetic cationic peptide, Antimicrob. Agents Chemother. 56 (2012) 2696–2704.
- [27] S.-W. Luo, W. Wei, P. Yang, C.-M. Lai, Q.-j. Liang, Y. Liu, et al., Characterization of a CD59 in orange-spotted grouper (Epinephelus coioides), Fish Shellfish Immunol. 89 (2019) 486–497.
- [28] V. Pandey, R.A.H. Bhat, S. Chandra, R.S. Tandel, M.K. Dubey, P. Sharma, et al., Clinical signs, lethal dose and histopathological lesions in grass carp, Ctenopharyngodon idella experimentally infected with Edwardsiella tarda, Microb. Pathog. 161 (2021) 105292.
- [29] V.I. Lushchak, Environmentally induced oxidative stress in aquatic animals, Aquat. Toxicol. 101 (2011) 13–30.
- [30] J. Ma, X. Li, M. Cui, W. Li, X. Li, Negative impact of the imidazolium-based ionic liquid [C8mim] Br on silver carp (Hypophthalmichthys molitrix): long-term and low-level exposure, Chemosphere 213 (2018) 358–367.
- [31] A.M. Rizzo, P. Berselli, S. Zava, G. Montorfano, M. Negroni, P. Corsetto, et al., Endogenous antioxidants and radical scavengers, in: Bio-farms for Nutraceuticals: Functional Food and Safety Control by Biosensors, Springer, 2010, pp. 52–67.
- [32] Y.-C. Su, F. Jalalvand, J. Thegerström, K. Riesbeck, The interplay between immune response and bacterial infection in COPD: focus upon non-typeable haemophilus influenzae, Front. Immunol. 9 (2018) 2530.
- [33] J. Bruslé, G.G. i Anadon, The structure and function of fish liver, in: Fish Morphology, Routledge, 2017, pp. 77–93.
- [34] I. Choi, H. Son, J.-H. Baek, Tricarboxylic acid (TCA) cycle intermediates: regulators of immune responses, Life 11 (2021) 69.
- [35] K. Awad, A.S. Maghraby, D.N. Abd-Elshafy, M.M. Bahgat, Carbohydrates metabolic signatures in immune cells: response to infection, Front. Immunol. 13 (2022) 012000
- [36] H. Zhao, L.N. Raines, S.C.-C. Huang, Carbohydrate and amino acid metabolism as hallmarks for innate immune cell activation and function, Cells 9 (2020) 562.
- [37] L. Perrin-Cocon, O. Diaz, A. Aublin-Gex, P.-O. Vidalain, V. Lotteau, Reprogramming of central carbon metabolism in myeloid cells upon innate immune receptor stimulation, Immuno 1 (2021) 1–14.
- [38] S. Chashmniam, M. Ghafourpour, A.R. Farimani, A. Gholami, B.F.N.M. Ghoochani, Metabolomic biomarkers in the diagnosis of non-alcoholic fatty liver disease, Hepat. Mon. 19 (2019).

- [39] P. Yaqoob, P.C. Calder, Fatty acids and immune function: new insights into mechanisms, Br. J. Nutr. 98 (2007) S41–S45.
- [40] M.J. Bryson, M.L. Sweat, Is mevalonic acid a precursor of the corticosteroids? Arch. Biochem. Biophys. 96 (1962) 1–3.
- [41] S.P. Marin-Luevano, A. Rodriguez-Carlos, Y. Jacobo-Delgado, C. Valdez-Miramontes, J.A. Enciso-Moreno, B. Rivas-Santiago, Steroid hormone modulates the production of cathelicidin and human β-defensins in lung epithelial cells and macrophages promoting Mycobacterium tuberculosis killing, Tuberculosis 128 (2021) 102080.
- [42] D. Ben-Nathan, D.A. Padgett, R.M. Loria, Androstenediol and dehydroepiandrosterone protect mice against lethal bacterial infections and lipopolysaccharide toxicity, J. Med. Microbiol. 48 (1999) 425–431.
- [43] S. Jia, X. Li, W. He, G. Wu, Oxidation of energy substrates in tissues of fish: metabolic significance and implications for gene expression and carcinogenesis, in: Amino Acids in Nutrition and Health, Springer, 2021, pp. 67–83.
- [44] P. Li, Y.-L. Yin, D. Li, S.W. Kim, G. Wu, Amino acids and immune function, Br. J. Nutr. 98 (2007) 237–252.
- [45] M. Murugan, E.-A. Ling, C. Kaur, Glutamate receptors in microglia, CNS & Neurological Disorders-Drug Targets (Formerly Current Drug Targets-CNS & Neurological Disorders) 12 (2013) 773–784.
- [46] E. Kvaratskhelia, E. Maisuradze, N.G. Dabrundashvili, N. Natsvlishvili, E. Zhuravliova, D.G. Mikeladze, N-methyl-D-aspartate and σ-ligands change the production of interleukins 8 and 10 in lymphocytes through modulation of the NMDA glutamate receptor, Neuroimmunomodulation 16 (2009) 201–207.
- [47] A.G. Del Arroyo, A. Hadjihambi, J. Sanchez, E. Turovsky, V. Kasymov, D. Cain, et al., NMDA receptor modulation of glutamate release in activated neutrophils, EBioMedicine 47 (2019) 457–469.
- [48] Y. Valero, E. Chaves-Pozo, J. Meseguer, M.A. Esteban, A. Cuesta, Biological role of fish antimicrobial peptides, Antimicrobial Peptides 2 (2013) 31–60.
- [49] X. Chen, Y. Yi, C. Bian, X. You, Q. Shi, Putative antimicrobial peptides in fish: using zebrafish as a representative, Protein Pept. Lett. 27 (2020) 1059–1067.
- [50] M.D. Ganfornina, S. Do Carmo, J.M. Lora, S. Torres-Schumann, M. Vogel, M. Allhorn, et al., Apolipoprotein D is involved in the mechanisms regulating protection from oxidative stress, Aging Cell 7 (2008) 506–515.
- [51] E. Rassart, A. Bedirian, S. Do Carmo, O. Guinard, J. Sirois, L. Terrisse, et al., Apolipoprotein d, Biochimica et Biophysica Acta (BBA)-Protein Structure and Molecular Enzymology 1482 (2000) 185–198.
- [52] G. Perdomo, H.H. Dong, Apolipoprotein D in lipid metabolism and its functional implication in atherosclerosis and aging, Aging (Albany NY) 1 (2009) 17.
- [53] J.-h. Gao, J.-l. Zhao, X.-l. Yao, T. Tola, J. Zheng, W.-b. Xue, et al., Identification of antimicrobial peptide genes from transcriptomes in mandarin fish (Siniperca chuatsi) and their response to infection with Aeromonas hydrophila, Fish Shellfish Immunol. 144 (2024) 109247.
- [54] C.M. Press, Ø. Evensen, The morphology of the immune system in teleost fishes, Fish Shellfish Immunol. 9 (1999) 309–318.